Operation of Polycarbonate Projectiles in the Ram Accelerator

Timothy Elder

A thesis
submitted in partial fulfillment of the
requirements for the degree of

Master of Science in Aeronautics and Astronautics

University of Washington

2013

Program Authorized to Offer Degree: Aeronautics & Astronautics

University of Washington

Abstract

Operation of Polycarbonate Projectiles in the Ram Accelerator

Timothy Elder

Chair of the Supervisory Committee:
Professor Adam Bruckner
UW Aeronautics & Astronautics

The ram accelerator is a hypervelocity launcher with direct space launch applications in which a sub-caliber projectile, analogous to the center-body of a ramjet engine, flies through fuel and oxidizer that have been premixed in a tube. Shock interactions in the tube ignite the propellant upon entrance of the projectile and the combustion travels with it, creating thrust on the projectile by stabilizing a high pressure region of gas behind it. Conventional ram accelerator projectiles consist of aluminum, magnesium, or titanium nosecones and bodies. An experimental program has been undertaken to determine the performance of polycarbonate projectiles in ram accelerator operation. Experimentation using polycarbonate projectiles has been divided into two series: determining the lower limit for starting velocity (i.e., less than 1100 m/s) and investigating the upper velocity limit. To investigate the influence of body length and starting velocity, a newly developed "combustion gun" was used to launch projectiles to their initial velocities. The combustion gun uses 3-6 m of ram accelerator test section as a breech and 4-6 m of the ram accelerator test section as a launch tube. A fuel-oxidizer mix is combusted in the breech using a spark plug or electric match and bursts a diaphragm, accelerating the ram projectile to its entrance velocity. The combustion gun can be operated at modest fill pressures (20 bar) but can only launch to relatively low velocities (approximately 1000 m/s) without destroy-

ing the projectile and obturator upon launch. Projectiles were successfully started at entrance velocities as low as 810 m/s and projectile body lengths as long as 91 mm were used. The tests investigating the upper Mach number limits of polycarbonate projectiles used the conventional single-stage light-gas gun because of its ability to reach higher velocities with a lower acceleration launch. It was determined that polycarbonate projectiles have an upper velocity limit in the range of 1500-1550 m/s which is lower than that of magnesium projectiles.

TABLE OF CONTENTS

LIST OF FIGURES

ACKNOWLEDGMENTS

None of the research presented here could have been done without help from the ram lab assistants. Nate Swartz, Kevin Dimond, and Sergio Marquez were of great help in the low velocity series of experiments. Zac Clausing's assistance in many experiments has made my time in the lab much more productive and his initiative has allowed me to spend time writing this report. For this, I am very thankful. The skillful manufacturing of projectiles and other parts by Viggo Hansen and Robert Aaron was essential to the success of this project. There are many volunteers who have assisted in experimentation over the last few years and all of their hard work is deeply appreciated.

I would like to express my deepest thanks to Mark Russell for not only his support of this research but for his encouragement in my pursuit of this degree. His enthusiasm for the subject matter sparked my own interest in this field. Professor Carl Knowlen has been instrumental in making my years at UW incredibly valuable. His willingness to spend time educating me on all things ram has been essential in my development as an engineer and in the writing of this thesis.

Chapter 1

INTRODUCTION

The ram accelerator is a hypervelocity launcher developed at the University of Washington that operates on the same principles as a ramjet engine. A sub-caliber projectile, analogous to the center-body of a ramjet engine, flies through fuel and oxidizer that have been premixed in a tube. Shock interactions in the tube ignite the propellant upon entrance of the projectile and the combustion travels with it. This combustion region creates thrust on the projectile by stabilizing a high pressure region of gas behind it (see Figure 1.1) .

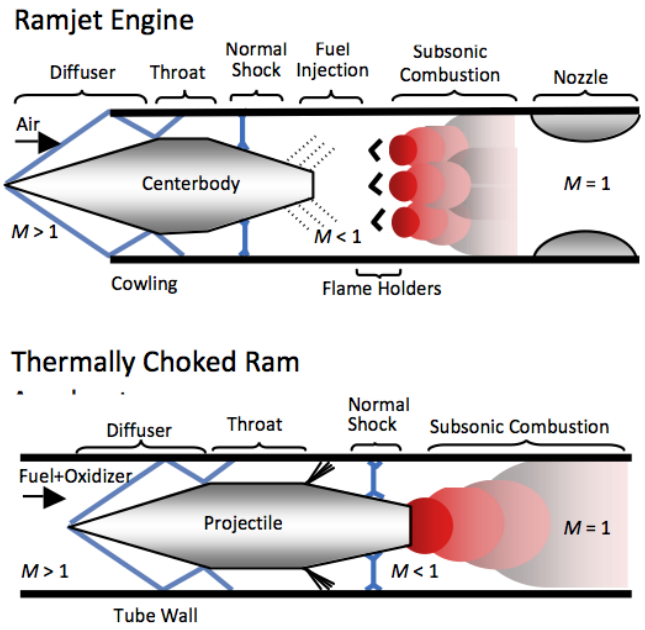

Figure 1.1: Ram accelerator vs. ramjet engine

Because the fuel and oxygen are pre-mixed, the propellant composition and pressure can be varied via staging to tailor the velocity and acceleration vs. distance profile of the projectile.[8] [9]

The position of the high pressure region immediately behind the projectile is the primary difference between the ram accelerator and a conventional gun. In a gun, the highest pressure is always in the breech which limits the upper velocity potential of a bullet to the speed of the free expansion of the driver gas (see Figure 1.2). Depending on the mode of operation, a ram accelerator projectile's upper limit is much

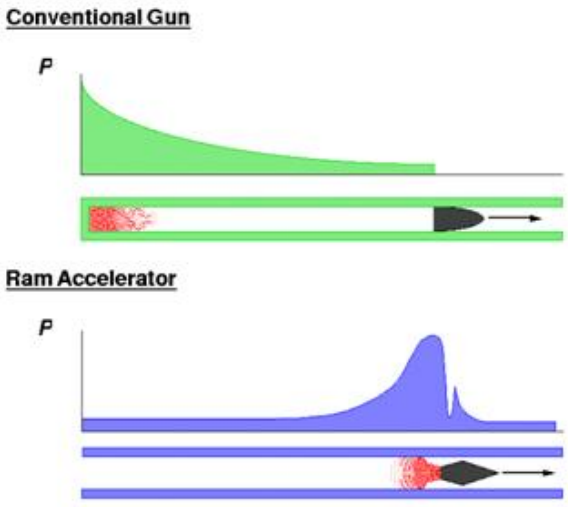

Figure 1.2: Pressure distribution in conventional gun and ram accelerator

higher. In the thermally choked ram accelerator mode in the subdetonative velocity regime, supersonic flow is maintained over the throat of the projectile and is brought to subsonic by a shock system on the back end of the projectile. The propellant burns behind the projectile, choking the flow and stabilizing the shock system. As the projectile velocity increases, the shock moves further down the projectile until it reaches full tube area. This point corresponds to the projectile traveling at the Chapman-Jouget (CJ) detonation velocity of the propellant and the theoretical zero-

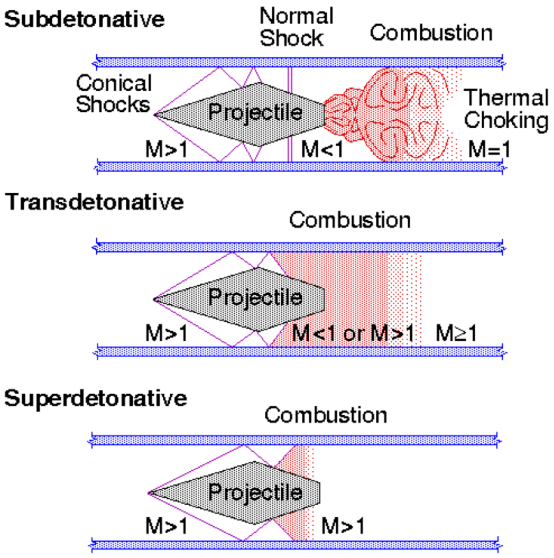

Figure 1.3: Modes of operation of the ram accelerator

thrust point. Experimental results agree well with theory based on the thermally choked mode up to a projectile velocity of about 85% the CJ velocity. At this point, however, the projectile's thrust reaches a minimum and begins to increase again, accelerating the projectile to velocities greater than the CJ velocity. This velocity regime (85%-105% CJ velocity) is referred to as transdetonative. The third regime is superdetonative in which projectiles travel at Mach numbers up to 8.5. In oblique detonation modes in this regime, supersonic combustion takes place entirely on the projectile body. The thrust in these modes is less than that in the thermally choked mode but the projectile can obtain higher velocities. See Figure 1.3 for a schematic of the subdetonative, transdetonative, and super detonative ram accelerator modes. This report investigates phenomena occurring in the subdetonative thermally choked mode. [3] [4]

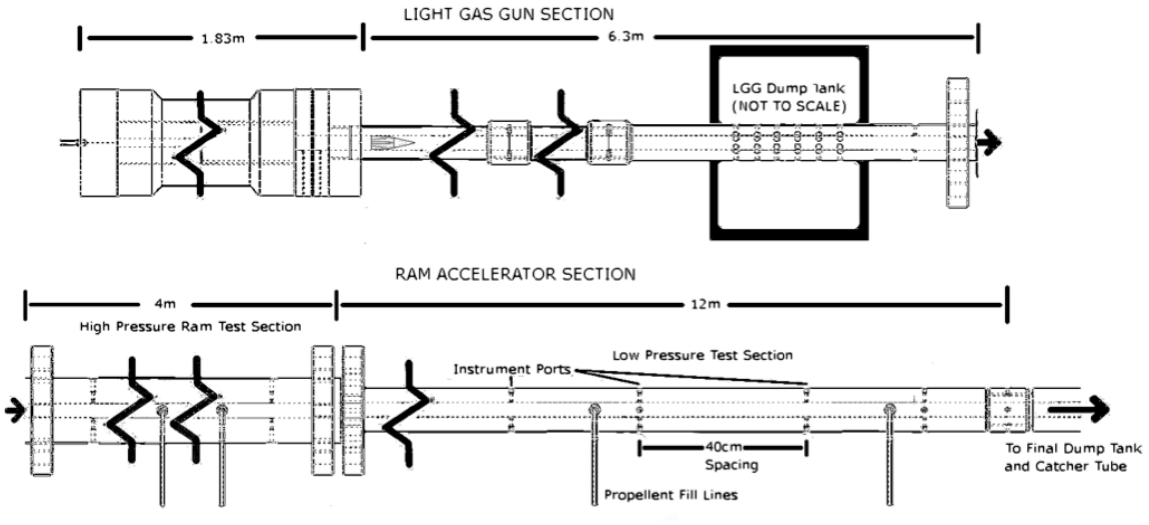

Figure 1.4: University of Washington ram accelerator facility

Facility

The University of Washington facility consists of a light-gas gun, an initial gas dump tank, ram accelerator test section, a final dump tank, and a projectile catcher tube (see Figures 1.4 and 1.5). The facility is 38-mm-bore. The light-gas gun is single stage, has a 2-m-long breech and 6-m-long launch tube. Maximum velocity from the light-gas gun is approximately 1300 m/s depending on the projectile mass and configuration. The end of the gas gun launch tube is a perforated vent tube and passes through the initial gas dump tank. During operation, this dump tank and the gas gun launch tube are evacuated to minimize precursor shock waves in front of the projectile. The driver gas from the gas gun can expand through the perforations in the vent tube, mitigating its effects on the starting process in the ram accelerator. [20]

The ram accelerator test section is comprised of 9 tubes (seven 2-m-long and 2 1-m-long) for a total length of 16 m. Diaphragms at the entrance and exit of the section contain a premixed oxidizer-fuel mixture. Maximum fill pressure in the ram

Figure 1.5: University of Washington ram accelerator facility view from final dump tank

accelerator tubes is limited to about 75 bar to accommodate pressure pulses that are present during operation. There are four fill ports along the test section through which oxidizer, fuel, and diluent are filled simultaneously. Multiport instrumentation stations (2-4 ports) are spaced along the length of the tube at 42 locations. Piezoelectric pressure transducers (model PCB 119A and 119B) monitor the wall pressure allowing for diagnosis of unsuccessful starts and tracking of projectile velocities. Electromagnetic transducers, consisting of a copper coil wrapped around a polycarbonate core and inserted into a stainless steel body, track the position of a magnet onboard the projectile and provide a time-postion history of the shot. [6] [2]

At the end of the ram accelerator test section is a 0.76-m-long drift tube that enters the final dump tank. The projectile exits the drift tube, flies in free-flight through the dump tank, and enters a catcher tube on the far side of the dump tank. The catcher

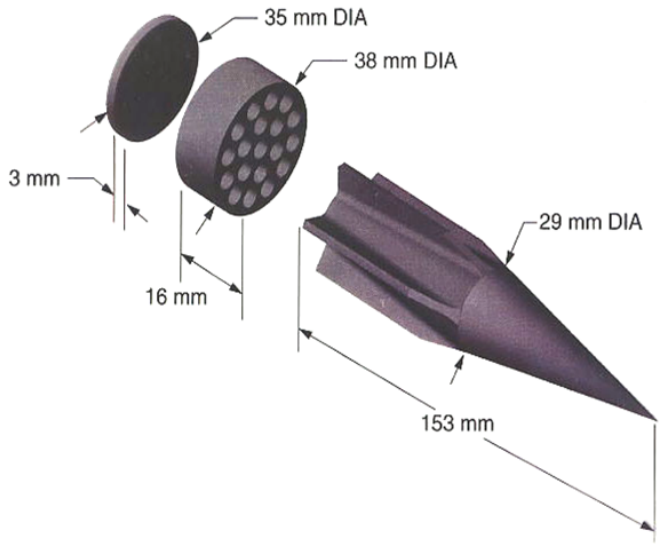

Figure 1.6: Conventional projectile and obturator configuration

tube is packed with aluminum and steel scraps interspaced with rug remnants. This material decelerates the projectile before the end of the catcher tube and dump tank.

The defining geometry characteristics of a ram accelerator projectile are nose cone angle, throat diameter, number of fins, and projectile material. The conventional ram accelerator projectile used in the University of Washington facility has a 12.5° nose cone half-angle, 29-mm-throat, 4-5 fins, and is made from aluminum, magnesium, or titanium (see Figure 1.6). The mass of the projectile typically falls in the range of 60-85 gm. In addition, a full-caliber obturator and disk combination is used to prevent blow by in the initial gun launch. The obturator also aids in the starting process of the ram accelerator by creating a region of subsonic flow behind the projectile throat.

Velocities of up to 2.7 km/s have been reached in the University of Washington ram accelerator. Entrance velocities as low as 690 m/s have been demonstrated in successful ram starts. In the subdetonative velocity regime, four different start outcomes have been observed: successful start, wave fall off, sonic diffuser unstart, and wave unstart. In a successful start, supersonic flow is maintained over the throat

(minimum flow area) of the projectile, the propellent ignites, and a shock system is stabilized on the back of the projectile, causing it to accelerate. In a wave fall off, the Mach number of the projectile is sufficient for the diffuser to gas dynamically start but the propellant does not ignite; the diffuser is gas dynamically started when the projectile is traveling above the minimum supersonic velocity at which the diffuser can accept the incoming mass flow rate (i.e., able the point where the Mach number is 1 in the throat region). If the propellant does not ignite, then the projectile coasts and decelerates at supersonic velocity. Various factors contribute to this result including excessive diluent, insufficient obturator mass, and insufficient projectile velocity. In the case of a sonic diffuser unstart, conditions at entrance of the test section do not allow for the diffuser to gas dynamically start. The diffuser cannot accept the incoming mass flow rate and thus the projectile throat flow area becomes choked (Mach = 1) which results in it pushing a normal shock wave ahead of the projectile, thereby, increasing the pressure on the projectile nose. A sonic diffuser unstart can be caused by too large a projectile diameter (i.e., too small a throat flow area) or insufficient projectile Mach number. A wave unstart occurs under conditions where the diffuser starts, the propellant is ignited behind the projectile, but a shock wave is then driven over the projectile and causes the diffuser to unstart. If the propellant mixture is reactive enough and the Mach number is high enough, the shock can ignite the propellant, resulting in a detonation wave ahead of the projectile. Upon its immediate formation, the detonation wave can be driven by the projectile to velocities in excess of the Chapman Jouguet speed, causing an intense pressure spike. Factors that cause a wave unstart include excessive propellant heat release, excessive obturator mass, and insufficient projectile diameter (i.e., too large a throat flow area). See Figure 1.7 for an example of the pressure waveform shape of a successful ram shot versus an unstart. [19] [15]

Polycarbonate projectiles are of interest in ram accelerator operation for several reasons. In large scale applications (i.e., direct space launch), it is likely that struc-

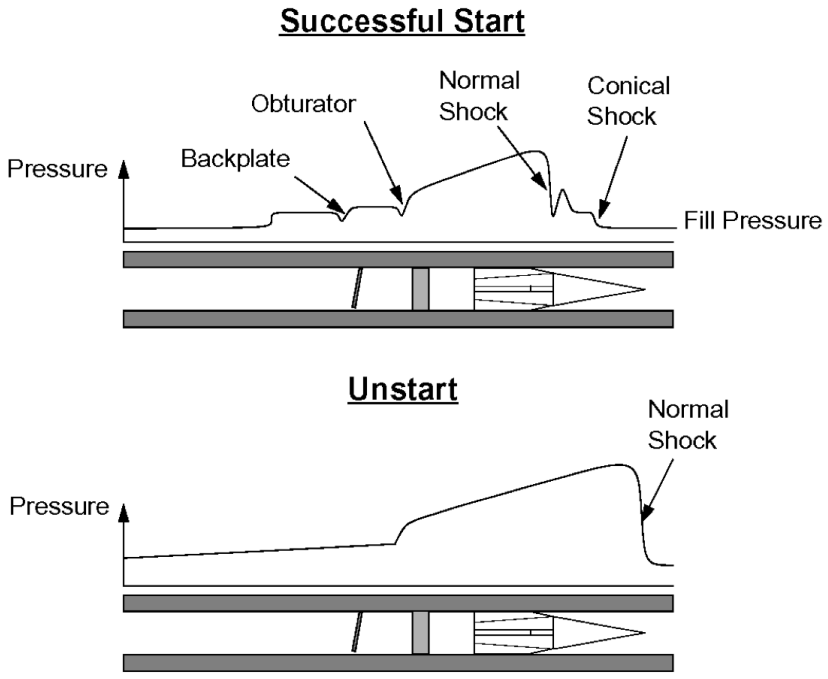

Figure 1.7: Pressure traces of a successful start vs. an unstart

tural limitations of the ram accelerator tube will limit fill pressures to moderate levels (< 35 bar). Thus, it is desirable that the aeroshell of the projectile be as light as possible to maximize its payload capacity. In addition, polycarbonate projectiles are of interest for experiments taking place at the current University of Washington facility. A low mass and easily manufactured projectile reduces the cost of experiments. This investigation of polycarbonate projectiles in the ram accelerator is divided into two series: low velocity starting and upper velocity limit. All of the experiments presented in this report take place in the subdetonative velocity regime.

Chapter 2

THEORY

Typical ram accelerator propellants utilize methane, hydrogen, or ethane as fuel, oxygen as oxidizer, and nitrogen, carbon dioxide, or excess fuel as diluent. Two pertinent characteristics of a propellant mixture are its sound speed and heat release. A given mixture has a Mach number range of operation. Depending on the sound speed, this Mach number range can correspond to different projectile velocities. The heat release of a propellant is defined by the non dimensional value Q where Q = $\Delta q/C_p T$. Q is only comparable within a given propellant class (i.e., same fuel, oxidizer and diluent) but not across different types of gases. Note also that Q is a function of Mach number. For ease of comparison, the Q value at the CJ Mach number is used to define a mixture. The conventional mixture for a projectile entering the test section at 1150 m/s is 2.7CH4 + 2O2 + 5.8N2. [16]

An expression for the non dimensional thrust on a projectile during thermally choked operation can be derived based on a "black box" control volume (see Figure 2.1). It is referred to as a black box control volume because the derivation does not depend on projectile geometry, only the gas conditions at the entrance and exit of the control volume. [3] [10]

The derivation starts with conservation equation for continuity, momentum, and energy (Equations 2.1-2.3):

$$\rho_1 u_1 A_1 = \rho_2 u_2 A_2 \tag{2.1}$$

$$P_1 A_1 + \rho_1 A_1 u_1^2 + F = P_2 A_2 + \rho_2 A_2 u_2^2 \tag{2.2}$$

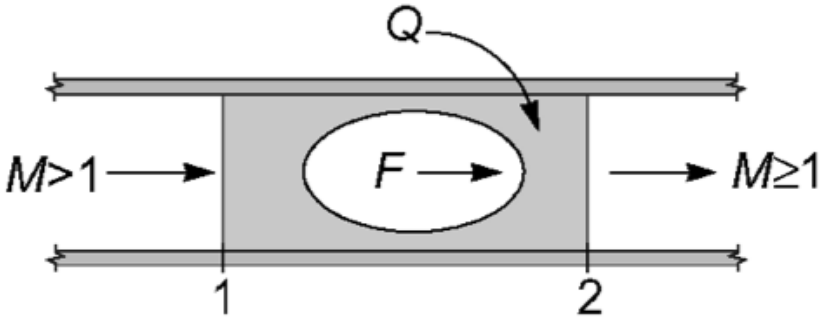

Figure 2.1: Control volume used for thrust derivation

$$h_1 + \frac{u_1^2}{2} + \Delta q = h_2 + \frac{u_2^2}{2} \tag{2.3}$$

Also used are the equation of state for an ideal gas and the equations of the speed of sound, Mach number, and gas constant for a gas (Equations 2.4-2.7):

$$P = \rho RT \tag{2.4}$$

$$a = \sqrt{\gamma RT} \tag{2.5}$$

$$M = \frac{u}{a} \tag{2.6}$$

$$R = c_p - c_v \tag{2.7}$$

Starting with the momentum equation (Equation 2.2), nondimensionalizing the force term F with $P_1 A_1$, setting $A_1 = A_2$, and applying Equation 2.6, the following is obtained

$$\frac{F}{P_1 A} = \frac{P_2}{P_1} - 1 + \frac{\rho_2 M_2^2 a_2^2}{P_1} + \frac{\rho_1 M_1^2 a_1^2}{P_1} \tag{2.8}$$

After applying Equations 2.5 and 2.4 with some algebraic manipulation, an expression for non dimensional thrust is,

$$\frac{F}{P_1 A} = \frac{P_2}{P_1}(1 + M_2^2 \gamma_2) - (1 + M_1^2 \gamma_1) \tag{2.9}$$

Now starting from the continuity equation (Equation 2.1), after applying the same equations and assumptions, the following is obtained

$$\frac{P_1}{R_1 T_1} M_1 \sqrt{\gamma_1 R_1 T_1} = \frac{P_2}{R_2 T_2} M_2 \sqrt{\gamma_2 R_2 T_2} \tag{2.10}$$

Some algebraic manipulation yields

$$\frac{P_2}{P_1} = \frac{M_1}{M_2} \frac{\sqrt{R_2 T_2 \gamma_1}}{\sqrt{R_1 T_1 \gamma_2}} \tag{2.11}$$

Finally, starting from the energy equation (Equation 2.3), the heat release Δq is nondimensionalized using $Q = \frac{\Delta q}{c_{p1} T_1}$:

$$\frac{h_1}{c_{p1} T_1} + \frac{u_1^2}{2 c_{p1} T_1} + Q = \frac{h_2}{c_{p1} T_1} + \frac{u_2^2}{2 c_{p1} T_1} \tag{2.12}$$

The same equations for sound speed and Mach number are applied (Equations 2.5 and 2.6):

$$\frac{h_1}{c_{p1} T_1} + \frac{M_1^2 \gamma_1 R_1 T_1}{2 c_{p1} T_1} + Q = \frac{h_2}{c_{p1} T_1} + \frac{M_2^2 \gamma_2 R_2 T_2}{2 c_{p1} T_1} \tag{2.13}$$

Applying the relation $R = \frac{c_p(\gamma - 1)}{\gamma}$ and some algebraic manipulation yields

$$\frac{h_1}{c_{p1} T_1} + \frac{M_1^2 (\gamma_1 - 1)}{2} + Q = \frac{h_2}{c_{p1} T_1} + \frac{M_2^2 (\gamma_2 - 1)}{2} \tag{2.14}$$

which can be simplified to

$$\frac{T_2}{T_1} = \frac{c_{p1}}{c_{p2}} \left[\frac{\frac{h_1}{c_{p1}T_1} + \frac{M_1^2(\gamma_1 - 1)}{2} + Q}{\frac{h_2}{c_{p2}T_2} + \frac{M_2^2(\gamma_2 - 1)}{2}} \right] \tag{2.15}$$

Equations 2.11 and 2.15 are substituted into Equation 2.9 to obtain

$$\frac{F}{P_1 A} = \frac{M_1}{M_2} \sqrt{\frac{R_2\gamma_1}{R_1\gamma_2} \frac{c_{p1}}{c_{p2}} \left[\frac{\frac{h_1}{c_{p1}T_1} + \frac{M_1^2(\gamma_1 - 1)}{2} + Q}{\frac{h_2}{c_{p2}T_2} + \frac{M_2^2(\gamma_2 - 1)}{2}} \right] (1 + M_2^2\gamma_2)} - (1 + M_1^2\gamma_1) \tag{2.16}$$

Applying the relation $R = \frac{c_p(\gamma - 1)}{\gamma}$ and simplifying yields

$$\frac{F}{P_1 A} = \frac{M_1}{M_2} \frac{\gamma_1}{\gamma_2} \sqrt{\frac{\gamma_2 - 1}{\gamma_1 - 1} \left[\frac{\frac{h_1}{c_{p1}T_1} + \frac{M_1^2(\gamma_1 - 1)}{2} + Q}{\frac{h_2}{c_{p2}T_2} + \frac{M_2^2(\gamma_2 - 1)}{2}} \right] (1 + M_2^2\gamma_2)} - (1 + M_1^2\gamma_1) \tag{2.17}$$

At this point a few assumptions simplify the expression. For the case of the thermally choked mode, $M_2 = 1$. In addition, if c_p is assumed not to vary significantly then $h = c_p T$ and $\gamma_1 = \gamma_2$. Applying this assumptions, we get

$$\tau = \frac{F}{P_1 A} = M_1 \sqrt{2(\gamma + 1)(1 + \frac{\gamma - 1}{2} M_1^2 + Q)} - (1 + M_1^2\gamma) \tag{2.18}$$

where τ is the nondimensional thrust. Whereas this expression provides a qualitative sense of the performance of the ram accelerator, the assumptions made prevent it from accurately predicting the performance. To accomplish this, a computer code has been written that calculates the enthalpy h from tabulated data. The thermodynamic properties of the exit of the control volume are calculated as a series of quasi-steady solutions and are used to calculate the heat addition to control volume (known thesis). Iterating the thrust equation as the Mach number M_1 increases provides a solution

of the variation of thrust with increasing Mach. This program can accurately predict the performance of the ram accelerator for velocities below the Chapman Jouget Detonation Velocity. [10] [14] [3]

Chapter 3
EXPERIMENTAL SETUP

3.1 Initial Launcher

For the low velocity starting tests, a new initial gun pre-launcher was developed based on a combustion wave cycle. The breech consisted of the first 3 to 6 m of the ram accelerator test section. The entry of the ram accelerator was closed off using a thin circular plate of steel or aluminum in place of a diaphragm. The other end of the breech was closed with a 0.36 mm Mylar diaphragm. On the upstream side of the breech, an electric match or spark plug threaded into an instrumentation port initiated the combustion wave. The projectile was loaded downstream of the Mylar diaphragm. The next 3-6 m of ram test section was evacuated and used as a launch tube for the combustion gun. Finally the remaining length of the ram tube was used as ram accelerator test section and was sealed on both ends with diaphragms. A key distinction between use of the combustion gun and use of the conventional light gas gun is the absence of a dump tank before the ram test section. To prevent excessive build up of precursor shock waves ahead of the projectile in the launch tube and potential pre-break of the ram diaphragm, it was essential that the launch tube be evacuated to as low a vacuum as possible [20]. In addition, several diaphragms were stacked at the ram test section entrance to help further prevent diaphragm pre-break.

A method of characteristics gas gun code was developed as a first order attempt to predict the performance of the combustion gun. Its accuracy was verified by performing an experiment with an inert gas. Helium was loaded into the breech until the Mylar diaphragm burst and the velocity of a polycarbonate slug was recorded. In Figure 3.1 the code's agreement with experimental results can be seen.

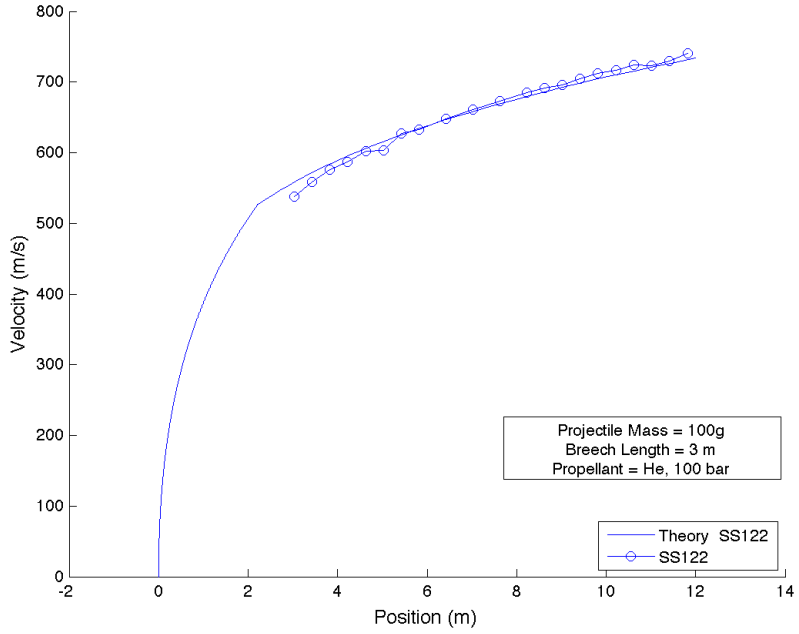

Figure 3.1: Comparison of method of characteristics code with inert gas slug shot experiment

An attempt was made to make the method of characteristics gas gun code predict the behavior of the combustion gun. First, this was modeled by assuming that the entire gas in the breech takes on the characteristics of the post-combustion fuel-oxidizer products. For example, as predicted by the NASA Chemical Equilibrium with Applications code, the combustion pressure ratio for $4H_2+1O_2+0.2He$ is 19.1 and the temperature ratio is 12.6. Applying these ratios in the method of characteristics code to the fill pressure and temperature of a combustion gun shot resulted in a predicted velocity much higher than than the experimental result. This is not surprising because the wave dynamics of a combustion gun shot are much more complicated than those of an inert gas gun. To compensate for this, the combustion parameters were once again used but the breech length entered into the code was shortened until the predicted velocity matched with the experimental velocity. The motivation for this approach

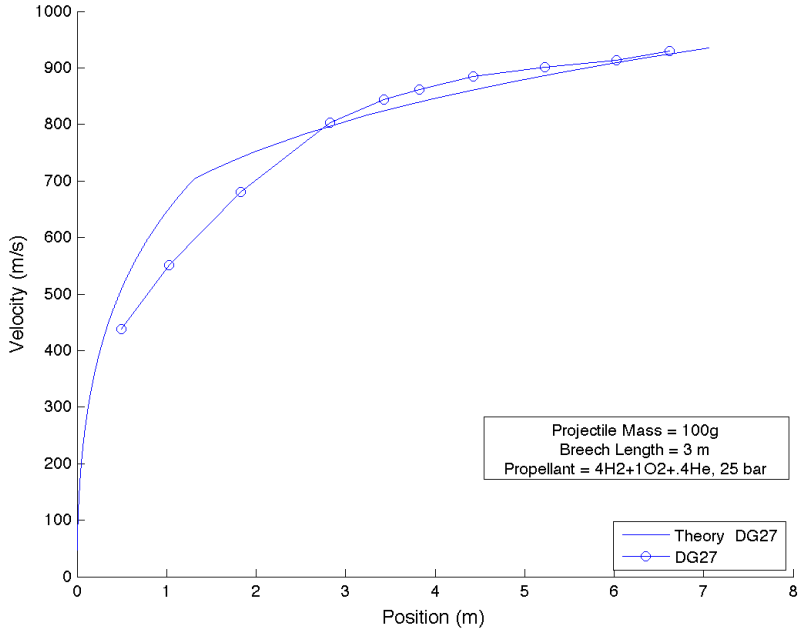

Figure 3.2: Comparison of method of characteristics code with combustion gun experiment using an effective breech length of 0.55m (actual breech length 3 m)

was that an "effective breech length" might be determined for the combustion gun. In Figure 3.2, the results of this attempt are plotted. Although the theory follows the experimental results somewhat, the effective breech length used in this analysis did not predict results for different mass projectiles and different breech fill pressures.

After the shortcomings of the method of characteristics code were realized, performance of the combustion gun was predicted by scaling from reference shots. The majority of experiments used $4H_2 + 1O_2 + 0.44$He for the combustion mixture. The fill pressure required for each shot was scaled from the reference data. These data were obtained through polycarbonate piston calibration shots. During the course of this calibration, an interesting lack of dependence of peak gun velocity on breech length was observed (see Figure 3.3). This observation confirms that wave dynamics of a combustion gun are inherently different from those in a conventional light gas

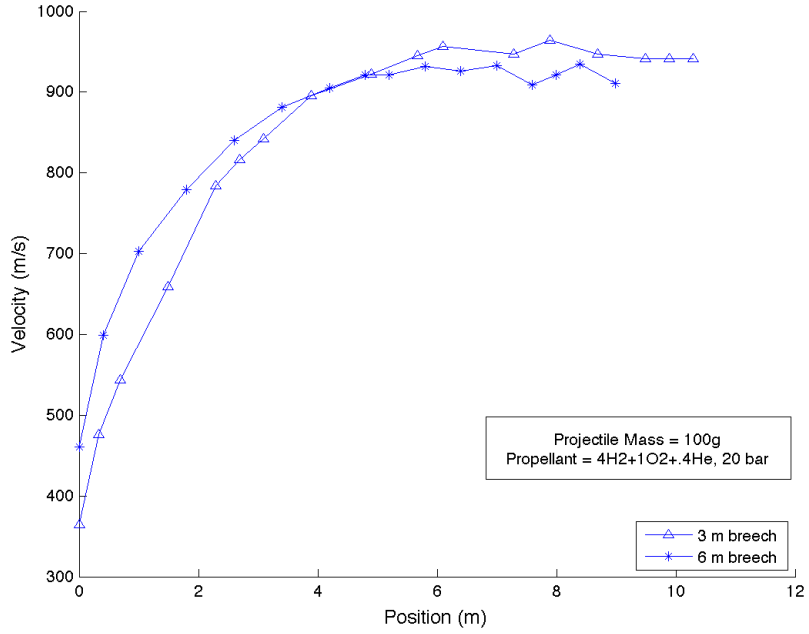

Figure 3.3: Comparison of piston combustion gun shots with varying breech lengths

gun in which breech length plays a significant role in maximum projectile velocity. For example, in Figure 3.4 the different predicted velocities of light gas guns with 3 and 6 m breeches can be seen. Furthermore, this allowed for the combustion gun breech to be shortened to 3 m for ram accelerator testing without sacrificing performance, providing for a longer test section of tube. Despite this unintuitive result, a database of piston shots using the combustion gun was developed and provided a reliable reference for scaling fill pressures for a given velocity and projectile mass requirement.

Investigating the upper velocity limits of polycarbonate projectiles required a higher entrance velocity than could be provided by the combustion gun as described above. So for these tests, two initial launcher guns were used.

First, the light gas gun breech was modified for use as a combustion gun. By doing this, the entire ram accelerator could be used as test section instead of several meters

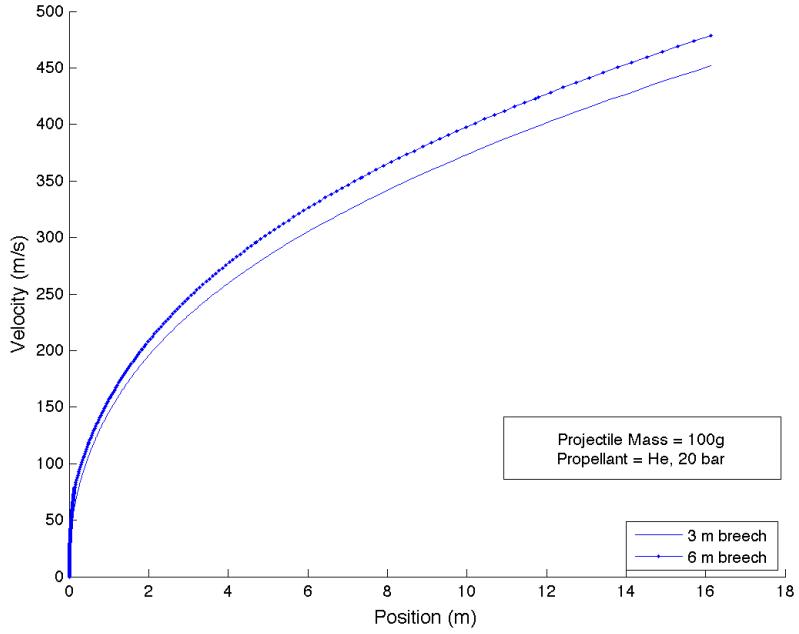

Figure 3.4: Method of characteristics code velocity predictions for 3 and 6 m breech lengths

being used for combustion gun breech and launch tube. It was also anticipated that the increased volume of and presence of chambrage in the light gas gun breech would lower the fill pressure required to obtain the 1100 m/s launch velocity.

Several piston reference shots and ram accelerator tests demonstrated that the required projectile velocity could not be achieved from modified combustion gun without exceeding the pressure rating of the light gas gun breech. Assuming a 20x pressure spike above the fill pressure during combustion, fill pressures had to be limited to 20 bar to prevent the breech from exceeding its 400 bar pressure rating. For this reason, the bulk of tests done for investigating the upper velocity limit of polycarbonate used the conventional light gas gun as a pre launcher. Not only could this configuration achieve higher inlet velocities to the ram accelerator but it also provided a softer launch, reducing the likelihood of destruction of the obturator.

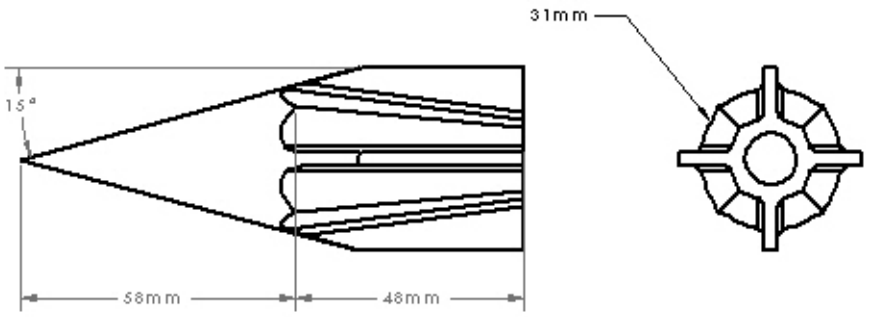

Figure 3.5: Magnesium projectile used for low velocity starting tests.

3.2 Projectiles

For a summary of polycarbonate projectiles used, see Table 3.1. The low velocity starting tests used three types of projectiles. All had a 15° nosecone angles and 31 mm diameter throats. These choices were motivated by the previous work in which it was determined that a "fatter" throat (larger maximum projectile diameter) aided in starting at low velocities (see Chapter 4). The first projectile was machined from magnesium and hollowed out to reduce the mass with a body length (throat to base) of 48 mm (see Figure 3.5). The mass was 63 g. The purpose of the magnesium projectiles was to establish a control result for comparison to behavior of the polycarbonate projectiles. Polycarbonate projectile Type A was identical in outer geometry to the magnesium projectile but was manufactured from polycarbonate and had three fins. This projectile had a threaded 13-mm-diameter hole drilled approximately 13 mm into the base. This hole was for a neodymium disk magnet to be held in place with a nylon set screw. Its mass was 56 g (see Figure 3.6). Another variation (Type B) had a solid base. Polycarbonate projectile Type C had a body length of 91 mm but was otherwise identical to the second variation of the second projectile. Its mass was 85

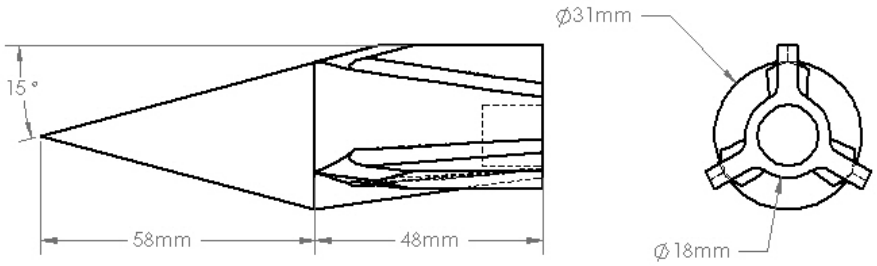

Figure 3.6: Type A polycarbonate projectile used for low velocity starting tests shown here with a magnet hole in the base. Type B was identical but had a solid base

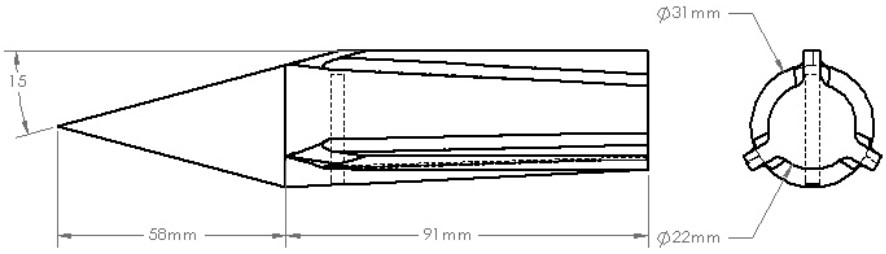

Figure 3.7: Type C polycarbonate projectile used for low velocity starting tests

g (see Figure 3.7).

The relatively high setback acceleration (5000-1000 g's) in the combustion gun required modification to the obturator design. The conventional obturator is perforated with 19 5.6 mm holes (see Figure 1.6). It was anticipated that this obturator would fracture under the loading in the combustion gun. The modified obturator used in these low velocity starting tests was solid, 38 mm in diameter and about 13 mm thick (see Figure 3.8). A chamfered base formed a "Bridgeman seal" that helped prevent blow-by in the launch process. Because the obturator was solid, the backplate used

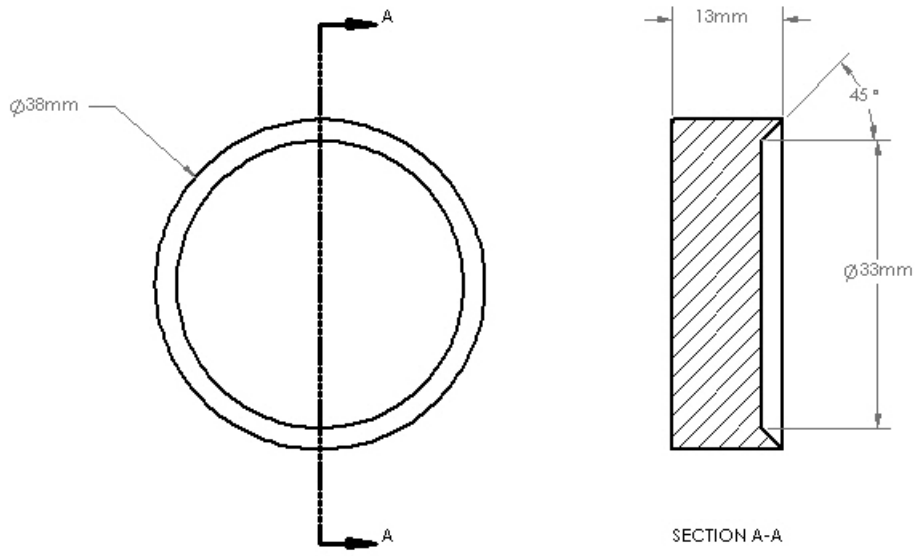

Figure 3.8: combustion gun obturator

in the conventional configuration was unnecessary.

Two main projectile variations were used in investigating the upper velocity limit of polycarbonate projectiles. First, magnesium projectiles with four fins, a 12.5° nosecone, a 29-mm-throat diameter, and a 71 mm throat-to-base length were used for comparison purposes. The projectile was drilled from the back to reduce weight as far as possible while still maintaining a sufficient nosecone wall thickness. Its mass was 65 g. This hole was also tapped to allow a nylon set screw to hold a neodymium magnet at the bottom of the hole. This design of projectile has had excellent repeatability in previous testing. The Type D polycarbonate projectile was identical in external geometry to the magnesium projectile. It did not have a hole from the base. Instead, the magnet was placed in a hole drilled into the side of the projectile just behind the throat. It had a mass of 62 g. See Figure 3.9 for a schematic of the polycarbonate and magnesium projectile used in these tests.

In addition to these projectiles, several other variations were shot when using the

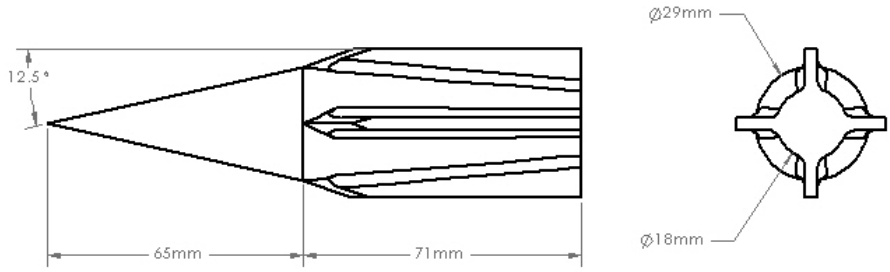

Figure 3.9: Type D polycarbonate projectile used for upper velocity limit tests, shown here without magnet hole. The magnesium projectile for the upper velocity limit tests was identical in outer geometry.

combustion gun with light gas gun breech. These projectiles were leftovers from the low velocity test series and had features such as 91 mm body length, 3 fins, 31 mm throat, and 15° nosecones.

Most of the shots in the upper velocity limit testing used conventional perforated obturators and solid polycarbonate disks for launching. Past experiments have showed the widest range of operation with this obturator configuration. For the tests in which the combustion gun was used, solid obturators of the same design as in the low velocity starting tests were initially used.

All projectiles were manufactured using a 3- or 4-axis CNC mill and manual or CNC lathes.

Table 3.1: Summary of Polycarbonate Projectiles

Type	Material	Mass (g)	Throat diameter (mm)	Body length (mm)	Nosecone angle	# Fins	Task	Magnet Position
A	Poly carbonate	56	31	48	15°	3	Low velocity starting	Base
B	Poly carbonate	56	31	48	15°	3	Low velocity starting	Throat
C	Poly carbonate	85	31	91	15°	3	Low velocity starting	Throat
D	Poly carbonate	62	29	71	12.5°	4	Upper velocity limit	Throat

Chapter 4

LOW VELOCITY STARTING EXPERIMENTS

Low velocity starting is of interest in ram accelerator operation to decrease the burden on the initial pre-launcher and to take full advantage of the ram accelerator. For example, in space launch applications it allows launch of projectiles containing g-sensitive payloads. The ram accelerator acceleration profile can be tailored by limiting the fill pressure, but most pre-launchers (e.g., powder guns, light gas guns) subject projectiles to very high accelerations (launch setback). By decreasing the velocity demand on the initial pre-launcher, this peak setback acceleration can be decreased [1].

A successful start in the ram accelerator requires that supersonic flow be maintained over the throat of the projectile. This condition creates one lower bound for low velocity starting. This can be obtained by adjusting several parameters of the projectile geometry and the ram accelerator configuration. The primary method of maintaining this flow over the projectile is simply ensuring that the projectile inlet velocity is sufficiently high for a given throat diameter and propellant composition. Assuming isentropic flow, this value for velocity can be determined from the relation

$$\frac{A_2}{A_1} = \frac{M_1}{M_2} \left(\frac{1 + [(\gamma - 1)/2] M_2^2}{1 + [(\gamma - 1)/2] M_1^2} \right)^{(\gamma+1)/2(\gamma-1)} \tag{4.1}$$

where A_1 is the full tube area of the ram accelerator and A_2 is the minimum flow area over the throat of the projectile. Alternatively, for a given velocity and propellant, the throat diameter ensuring supersonic flow can be calculated. Similarly, the required propellant acoustic speed can be determined for a given velocity and throat diameter. Since the objective is to successfully start the ram accelerator at as low a velocity as

possible, a small throat diameter (large throat flow area) and low acoustic speed will aid in maintaining supersonic flow over the throat.

Another requirement for a successful start is that the propellant ignites and stabilizes behind the projectile. Propellant ignition depends heavily on its compression as it passes through the conical shocks caused by the nose cone and throat flow contraction. For a low velocity experiment, all else the same, the conical shocks are weaker than in a higher velocity shot. Thus, the propellant experiences less compression. To compensate for this, projectile geometry can be altered to increase the compression and a more energetic propellant can be used. [17] [19] [15]

In Reference [17] efforts were undertaken to determine low velocity starting techniques. The original ram accelerator projectile used an onboard gunpowder ignitor system to aid in the starting process. A successful start was obtained at 710 m/s in a mixture of CH_4+$2O_2$+$5.6CO_2$ using a projectile with a 12.5° nosecone angle and a 29-mm-throat. The present investigation, however, does not utilize the gunpowder ignitor so the focus will be on past experiments without this addition. Attempting to replicate this result at 780 m/s with a 29-mm-diameter projectile with a 10° nosecone without an ignitor were not successful. It was found that a 0.1 mole increase in the amount of CO_2 in the mixture changed the outcome from a wave unstart to a wave fall off. It was concluded that this projectile and propellant configuration could not reliably start. Tests with projectiles with a 15° nosecone yielded similar results.

In an effort to increase projectile Mach number, an ethane-based propellant mixture was investigated. This series of mixtures had an acoustic speed of approximately 285 m/s, whereas the methane-base mixtures had an acoustic speed of approximately 305 m/s. While the higher molecular weight of ethane decreases the acoustic speed of the mixture, a disadvantage of this mixture is that the vapor pressure of ethane is approximately 40 bar, thus limiting ram operation to below this pressure. A nominal projectile (15° nosecone, 29-mm-diameter) experienced a relatively narrow window of operation of 5.12-5.22 CO_2. Using a mixture of $1.5C_2H_6$ + $2O_2$ + $6.24CO_2$ and a

projectile with a 31 mm diameter (decreasing the open flow area around the projectile throat) resulted in the projectile driving 2 m through the entire stage. The one attempt to replicate this shot, however, resulted in a wave fall off [17].

In Reference [19] the effects of propellant, entrance Mach number, and projectile throat area on starting the ram accelerator in the subdetonative velocity regime were studied. Using a propellant range of $2.8CH_4 + 2O_2 + (4.5\text{-}7.5)N_2$ and an entrance Mach number of 2.8, a successful start was not achieved. The result changed from wave unstart to a wave fall off with a 5% change in heat release. Raising the Mach number to 2.9 broaded the operating envelope to a Q_{CJ} range of 4.4-5.3. No successful starts occurred using a propellant class of $CH_4/O_2/CO_2$. In a CH_4/O_2 propellant at a Mach number of 3.3, the Q_{CJ} range of operation was 5.0-5.3. In general, the authors determined that low propellant heat release Q and Mach number lead to wave fall-off outcomes. Furthermore, high Q causes wave unstarts. Interestingly, wave unstarts occur both below and above the functional Mach number range of a propellant. The authors propose the explanation that low Mach number projectiles cannot contain the combustion wave and high Mach number projectiles might initiate detonation ahead of the throat.

The effects of varying throat flow area were also studied in Reference [19]. The authors determined that for a constant Q and Mach number, a larger throat flow area cannot contain the shock system behind the throat. A larger throat flow area requires either a higher entrance Mach number or a lower Q to start successfully. In addition, a smaller throat flow area aids in starting and allows for more energetic propellants to be used. The lower limit for throat flow area is the sonic diffuser limit; as the throat flow area decreases, the minimum Mach number required to maintain supersonic flow over the throat increases. [19]

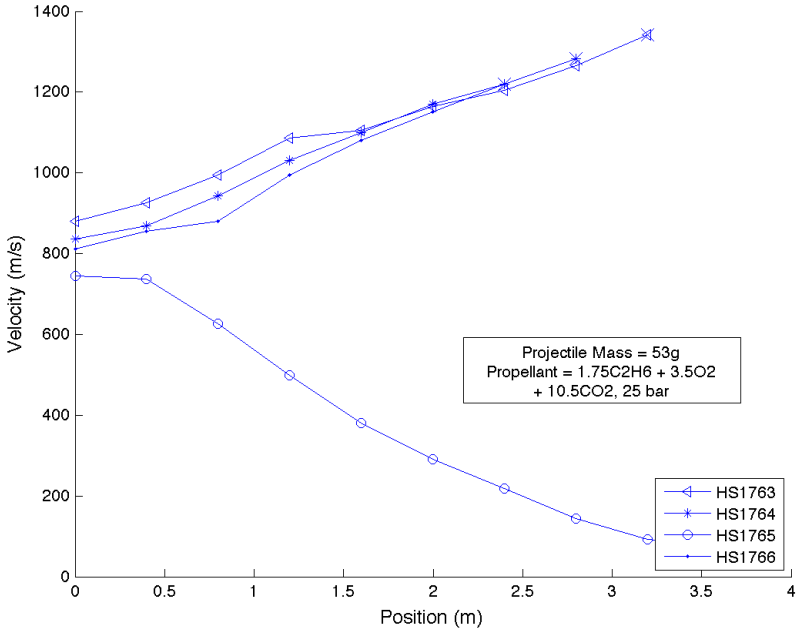

Figure 4.1: Velocity-distance data for 48-mm-long magnesium projectiles

4.1 Results

For a summary of all the experiments done in the low velocity starting series, see Appendix A. A reference configuration was found using the magnesium projectiles in a mixture of $1.75C_2H_6 + 3.5O_2 + 10.5CO_2$ with a fill pressure of 25 bar. As shown in Figure 4.1, projectiles with entrance velocities ranging from 810-870 m/s started and accelerated for at least 2.4 m while attaining a velocity incase of over 400 m/s. Lowering the entrance velocity to 750 m/s resulted in the projectile promptly unstarting. Thus the minimum starting velocity is between 750 and 810 m/s.

In Figure 4.2 selected data are presented for tests using Type A polycarbonate projectiles. These projectiles was initially unsuccessful in repeating the magnesium projectile results; the projectile experienced a wave fall off (HS1767). Attempts to make the propellant more energetic by removing CO_2 or excess fuel caused an abrupt

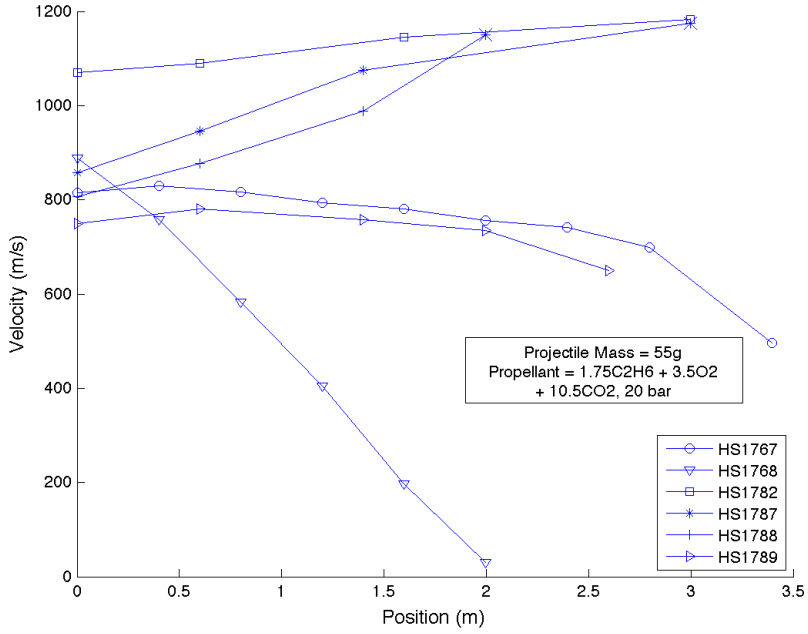

Figure 4.2: Velocity-distance data for Type A and B projectiles

transition from wave fall off to wave unstart in HS1768. Tests were then performed using a polycarbonate projectile of Type B with a solid base. The first solid base polycarbonate projectile ran for at least 3 m from 1070 m/s to 1180 m/s in a $1.75C_2H_6$ + $3.5O_2$ + $10.5CO_2$ at 20 bar fill pressure (HS1782). In these tests without magnets, pressure transducers were used in determining projectile position. Lowering the velocity to 860 m/s also resulted in a successful start with the projectile running to 1180 m/s over 3 m (HS1787). The velocity was then lowered further to 810 m/s in HS1788 which also successfully started, running to approximately 1150 m/s before unstaring 2 m into the test section. A projectile with an inlet velocity of 750 m/s resulted in a wave fall off followed by an unstart (HS1789).

Type C projectiles with a 91-mm-long body was tested in the $1.75C_2H_6$ + $3.5O_2$ + $10.5CO_2$ propellant at 20 bar with an inlet velocity of 860 m/s (HS1791, see Figure 4.3). The projectile experienced a wave fall off and coasted out of the test section.

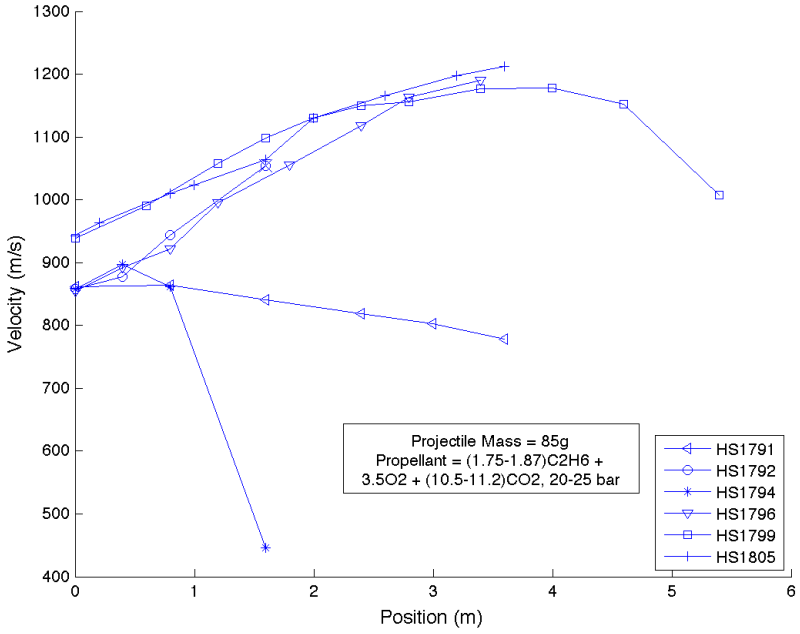

Figure 4.3: Velocity-distance data for Type C projectiles in ethane-based propellants

By increasing the fill pressure to 25 bar in HS1792, however, the projectile ran for 1.5 m to 1060 m/s before unstarting. Several repeats of the same experiment resulted in the wave falling off. Increasing the heat release of the propellant by removing 0.5 moles of CO_2 caused the projectile to promptly unstart in HS1794. In a repeat of the $1.75C_2H_6 + 3.5O_2 + 10.5CO_2$ test at 25 bar, the projectile ran out of the test section up to 1190 m/s in HS1796. In this sequence of tests, there were difficulties in obtaining repeatable results so a later test used a $1.87C_2H_6 + 3.5O_2 + 11.2CO_2$ propellant at 25 bar. Here, the projectile entered at 910 m/s and ran to 1180 m/s in 3 m before coasting at that velocity for 1 m and then unstarting (HS1799). In test HS1805 with an 6 m test section and the same propellant, a projectile entering at 950 m/s ran the through the entire test section, exiting at 1212 m/s.

A series of tests were also performed in a ethylene-based mixture (see Figure 4.4). Using the same Type C polycarbonate projectile, a mixture of $1.5C_2H_4 + 3O_2 +$

11.5CO_2 at 20 bar ran from 940 m/s to 1310 m/s over the 4 m test section in HS1814. In an effort to determine the upper velocity limit of the projectile and propellant

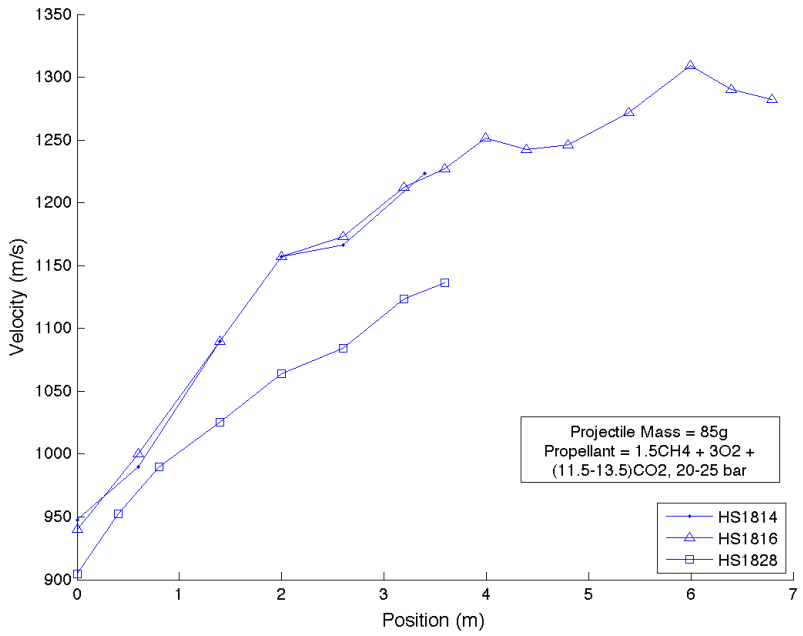

Figure 4.4: Velocity-distance data for Type C projectiles in ethylene-based propellants

configuration, the test section was increased to 8 m in length. In this case, the projectile promptly unstarted. To mitigate the potential for in accuracies in propellant filling in a relatively long 8 m test section, the stage was divided into two 4 m sections in the next test. The two stages were filled sequentially, assuring that the mixture in the first 4 m was identical to the mixture in the successful 4 m ethylene shot. This test (HS1816) was successful, with the projectile entering the 20 bar mixture at 940 m/s and driving through the entire 8 m test section to 1290 m/s. Once again, difficulties were encountered in obtaining repeatability for the ethylene based mixtures. In an effort to expand the operating window of the ram accelerator, several tests were performed with the 91 mm polycarbonate projectile using the conventional perforated obturator with disk in place of the solid obturator. After several shots to

adjust the chemistry, a projectile entering a $1.5C_2H_4 + 3O_2 + 13.5CO_2$ at 25 bar at 905 m/s ran through the 4 m test section to 1140 m/s (HS1828).

4.2 Comparison with Theory

Using an existing quasi-steady, one-dimensional, inviscid model of the thermally choked ram accelerator mode, experimental data could be compared to theory. In Figure 4.5, the velocity-distance data for a magnesium projectile are shown along with the corresponding data predicted by theory. Agreement with theory is observed past the transients associated with the ram accelerator starting process. In Figure 4.6

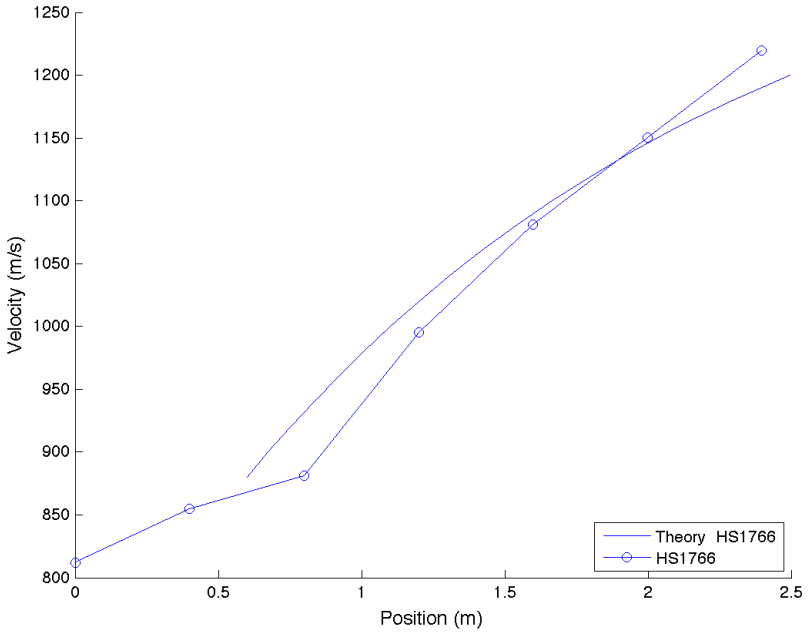

Figure 4.5: Theory vs experimental data for magnesium projectile in a $1.87C_2H_6 + 3.5O_2 + 11.2CO_2$ propellant

theory is compared to experimental data for polycarbonate projectiles. Here, the disagreement with theory is greater. In the experiment, the polycarbonate projectile seemed to follow the shape of the curve before the theory begins to over predict its

velocity.

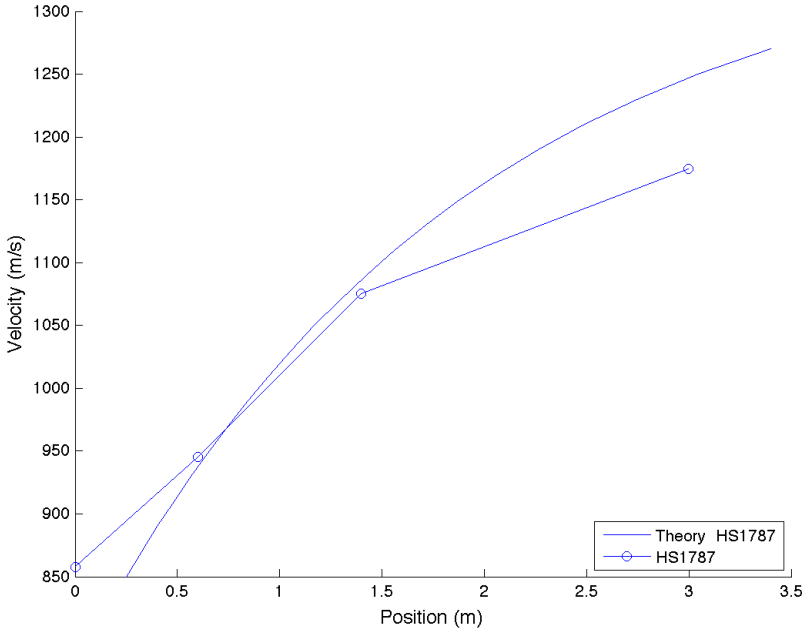

Figure 4.6: Theory vs experimental data for polycarbonate projectile in a $1.87C_2H_6 + 3.5O_2 + 11.2CO_2$ propellant

4.3 Discussion

In testing the Type A polycarbonate projectiles, it was determined that the hole for the magnet in the base of the projectiles prevented successful starting when attempting to replicate the magnesium shot. Recovered polycarbonate projectiles showed signs of buckling in the aft part of the body, manifested in a "bulge" part of the way up the body (see Figure 4.7). Anticipating that this could be causing the projectile to unstart, several projectiles were shot without the magnet hole in the base (Type B). Even though there were still signs of buckling, the Type B projectiles without the hole were able to start in the same mixture as the magnesium. There was no observed difference between the lower velocity limit between the polycarbonate and

Figure 4.7: Type A polycarbonate projectile after an unsuccessful shot with "bulge" on back end

magnesium. Both successfully started with an inlet velocity of 810 m/s and unstarted when entering at 750 m/s. There was, however, an difference observed in their upper velocity limits. Magnesium projectiles ran to velocities around 1300 m/s. The polycarbonate projectiles were not observed at velocities significantly higher than 1200 m/s. This difference in velocity potential also manifested itself in comparison to theory. The discrepancy between theory and experimental data that is present with polycarbonate projectiles but not with magnesium demonstrates an effect projectile material has on performance.

The largest difficulties in the low velocity start series were encountered with the Type C projectiles. Using conditions under which the Type B projectiles started, a Type C projectile experienced a wave fall off. Increasing the pressure in a subsequent test helped the propellent ignite and the projectile accelerated for 1.5 m before un-

starting. When the heat release of the mixture was increased by removing diluent, the projectile promptly unstarted. Eventually an operating condition was found at the $1.75C_2H_6 + 3.5O_2 + 10.5CO_2$ propellant and later at the $1.87C_2H_6 + 3.5O_2 + 11.2CO_2$ but there were difficulties in repeating obtaining repeatable results. The results from these tests imply that the longer body length impedes the ignition of the propellant. Due to the increased distance between the throat and obturator at the ram test section entrance, the propellant undergoes less compression. If the propellant is just on the verge of ignition then small variations in experimental conditions could cause inconsistent results. Perhaps the biggest source for variations for this test series was the flow control of the CO_2 delivery. Due to limitations in the electronic mass flow controllers, the CO_2 was controlled using a micro metered orifice. The mass flow rate was adjusted by opening and closing the orifice or by adjusting the upstream pressure of the orifice. Nonidealities in the orifice could lead to inconsistent delivery of the CO_2. The adiabatic cooling of the CO_2 in its gas supply cylinder could also be skewing results due to temperature and pressure variations of the flow upstream of the metering orifice. The tests using Type C projectiles in ethylene-based propellants displayed a similar inconsistency. Tests using a mixture of $1.5C_2H_4 + 3O_2 + 11.5CO_2$ at 20 bar resulted in both successful shots and unstarts.

Chapter 5

UPPER VELOCITY LIMIT EXPERIMENTS

In References [11] and [12], an envelope of operation was experimentally determined for two different propellants and projectile configurations. The propellants used were $2.8CH_4 + 2O_2 + XN_2$ at 25 bar and $2H_2 + 2O_2 + XCH_4$ at 50 bar where X allows for a variation in the diluent content and thus heat release of the mixture. The projectiles used were 64g 4-fin magnesium and 76.5g 5-fin aluminum, respectively. In these experiments, a projectile passed through a 2-m-long "starter stage" of $2.8CH_4 + 2O_2 + 5.87N_2$ to establish combustion. It then entered the test section. For a given class of propellant, the amount of diluent present was varied while the inlet velocity to the test section remained constant. The distance traveled and velocity achieved in the test section before unstart occurred was then observed. The results of the experiments were described on both a velocity-distance plot and a heat release-Mach number (Q-M) plot. For the nitrogen-diluted propellant, four limits of operation were observed. The first is a maximum heat lease Q beyond which the projectile will promptly unstart. On the other end is a minimum heat release below which ignition will not occur and the projectile will experience a wave fall off. The two other limits are functions of both heat release and Mach number. It was determined that there is a Q value for the nitrogen-diluted propellant that results in the projectile reaching the maximum Mach number. Below this Q value, the projectile travels further in the test section but accelerates more slowly, reaching a lower velocity. Above this Q value, the projectile accelerates more quickly but unstarts in a shorter distance. It was also observed that a significant portion of the operational envelope lay beyond the CJ detonation velocity of the mixture. The authors proposed that the Q limit on

the upper side of the peak Mach number could be attributed to gas dynamic effects. On the lower side of the peak Mach, the authors stated that the Q limit was more likely a consequence of material properties because of the projectiles long in-tube operation time. To further investigate this, a magnesium projectile with an aluminum nose was used in a test with a mixture that resulted in an unstart below the peak Mach number. This modified projectile drove more than 3 m further into the stage than the magnesium projectile and reached a velocity of 2160 m/s as opposed to 1990 m/s for the magnesium projectile. This results confirms that material effects play a role in the upper velocity limit of a given propellant.

A similar experiment was performed in the $2H_2 + 2O_2 + XCH_4$ propellant. By replacing the all-aluminum projectile with a titanium nose aluminum body projectile, a higher velocity was reached and the projectile drove out the entire test section. Furthermore, tests were performed with a Al-nose Ti-body projectile and an all Ti projectile. The aluminum nose projectile traveled as far into the test section as the all aluminum projectile but it did not reach as high a velocity because of its increased mass. The all titanium projectile exited the test section but also did not reach as high a velocity due to its increased mass. [11] [12].

In Reference [7] the effect of projectile material on transition to velocity regimes beyond subdetonative was investigated. A projectile manufactured from magnesium demonstrated transition to transdetonative mode by the end of the 16 m test section as indicated by pressure and luminosity transducers and deviation of performance from thermally choked theory. An aluminum projectile did not perform in the same manner. The pressure and luminosity transducers showed transition to transdetonative mode later than for the magnesium projectile. Also, its velocity history did not deviate from the theory. To isolate the effect of individual projectile components, a projectiles with aluminum nose and magnesium body and vice-versa were tested. The projectile with a magnesium body behaved similarly to the all-magnesium projectile in performance and transducer results. The opposite projectile (magnesium

nose, aluminum body) unstarted before transitioning to transdetonative mode. Before the unstart its performance was similar to the all-aluminum projectile. Also, a all-magnesium projectile coated in Teflon was tested. The Teflon seemed to prevent the projectile from completely transitioning to transdetonative mode and caused reduced velocity performance. The Teflon coated projectile followed the curve predicted by thermally choked theory.

The same experiments were then repeated at elevated fill pressures to examine the maximum performance of each projectile. In this series, the magnesium projectile unstarted 12 m into the test section. This premature unstart was thought to be caused by combustion taking place along the nose. The aluminum projectile, at these higher pressures, demonstrated similar performance as the magnesium projectile but drove out of the test section without unstarting. It is expected that the higher fill pressure helped the transition to transdetontive mode by increasing kinetic rates. The first hybrid projectile (aluminum nose and magnesium body) transitioned to transdetonative mode and drove out the entire test section but considerable deformation in the magnesium fins was observed. The other hybrid projectile (magnesium nose and aluminum body) entered transdetonative mode but unstarted before exiting the test section. Finally, the Teflon coated magnesium projectile took longer to reach transdetonative mode but the velocity data did deviate from theory at the 12 m mark. [7]

In Reference [13] the author performed experiments investigating the effect of material type in different parts of the projectile. The performance of projectiles with different combinations of aluminum and titanium nose and bodies was studied. A projectile with titanium nose and body exited the entire 16 m test section without unstarting. An all-aluminum projectile unstarted the soonest. A projectile with a titanium nose and aluminum body reached the same point in the tube as one with an aluminum nose and titanium body before unstarting. The former reached higher velocity, however, indicating that the projectile nose is most sensitive to material

effects. In an effort to find a robust nose that does not cost as much as titanium, magnesium projectiles were manufactured with different nose wall thicknesses. This change in geometry had no effect. The solid magnesium nose projectile drove just as far as one with the thinnest nose wall. The author proposed that this result showed that the nose tip is what deforms and causes unstarts; each magnesium projectile had a nose tip of the same shape and structure. [13]

In Reference [5] extensive work was done on calculating the heat transfer to projectile nosecones. It was predicted that aluminum nosecones will experience significant blunting which would have a negative effect on ram accelerator performance. The author showed that projectiles with nosecones made of other materials (i.e., titanium) are predicted to maintain structural integrity and obtain better performance.

5.1 Results

See Appendix B for a summary of upper velocity limit experiments. Several attempts were made to utilize the modified combustion gun with light gas gun breech to start in a $2.7CH_4 + 2O_2 + 5.8N_2$ propellant around 1100 m/s. In all experiments, the projectile experienced a prompt unstart and rapidly decelerated in the tube. After several failed tests using perforated obturators, solid obturators were used. It was eventually determined that sufficient projectile velocity could not be obtained in the combustion gun without destroying the obturator or exceeding the pressure rating of the light gas gun breech.

Results were much more consistent using conventional light gas gun initial launcher. The first shot to establish a baseline for performance used a magnesium projectile that had been shot previously but was recovered intact. This projectile had a 46 mm body but was otherwise identical to the magnesium projectile described previously. As shown in Figure 5.1, it entered the 3 m test section of $2.7CH_4 + 2O_2 + 5.8N_2$ at 25 bar at 1150 m/s and exited at 1440 m/s (HS1839). The subsequent shot (HS1840) repeated this configuration but added a 13 m second stage of $6CH_4 + 2O_2 + 2H_2 +$

.2He. Here the projectile entered the test section at 1190 m/s and exited the entire 16 m at 1770 m/s.

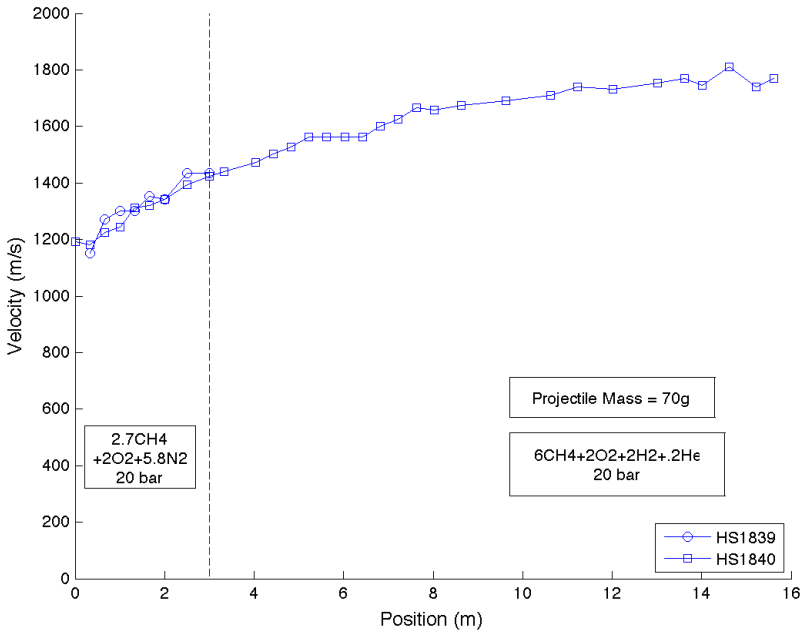

Figure 5.1: Velocity-distance data for magnesium projectiles using the light gas gun for upper velocity limit tests

Attempts to replicate these tests with polycarbonate projectiles were initially unsuccessful. In test HS1842, a polycarbonate projectile unstarted within 1 m of the entrance of the test section (see Figure 5.2). In an effort to reduce potential deformation of the projectile, the test was repeated at a 16 bar fill pressure (HS1843). Once again, this resulted in an unstart.

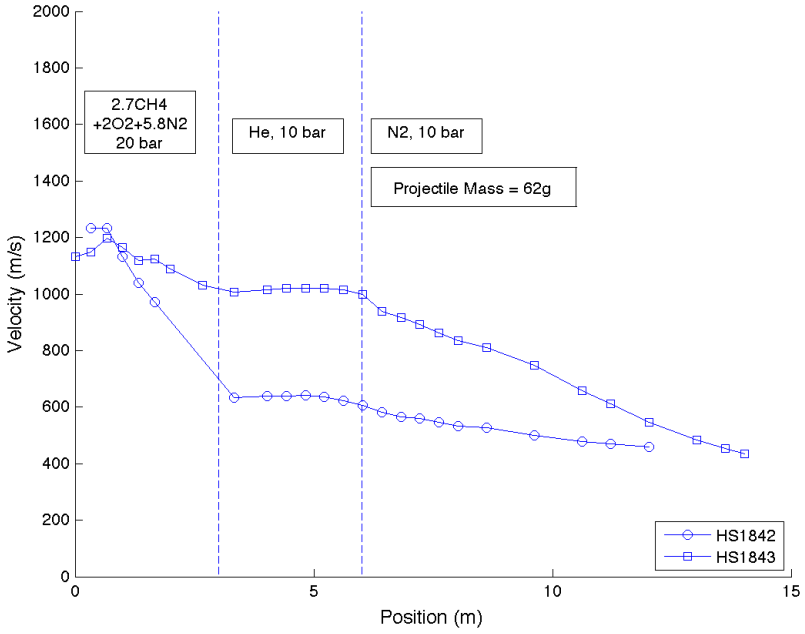

Figure 5.2: Velocity-distance data for Type D polycarbonate projectiles

Figure 5.3: Type D polycarbonate projectile caught with gas dynamic catcher

Both of these tests were performed with a "gas dynamic catcher" that allowed the projectile to decelerate without impacting any material and to be recovered intact. The gas dynamic catcher consisted of 3 m of ram tube after the test section being filled with helium and the remaining 10 m filled with nitrogen. The projectile unstarts in the helium section due to its acoustic speed and then rapidly decelerates in the

nitrogen. In both cases, the recovered projectile had no deformation that would obviously cause an unstart (see Figure 5.3).

Adjusting the propellant to $3.2CH_4 + 2O_2 + 5.8N_2$ at 25 bar resulted in the polycarbonate projectile driving out of the 3 m test section from a 1220 m/s to 1360 m/s in HS1844 (see Figure 5.4) . In order to determine the point at which the polycarbonate projectile unstarts, the test section was lengthened to 7 m. Once again, the projectile exited the test section, driving from 1200 m/s to 1570 m/s (HS1849). Lengthening the stage to 16 m resulted in the projectile running from 1230 m/s to 1510 m/s in 7 m before unstarting (HS1864). To investigate effects of nose tip deformation

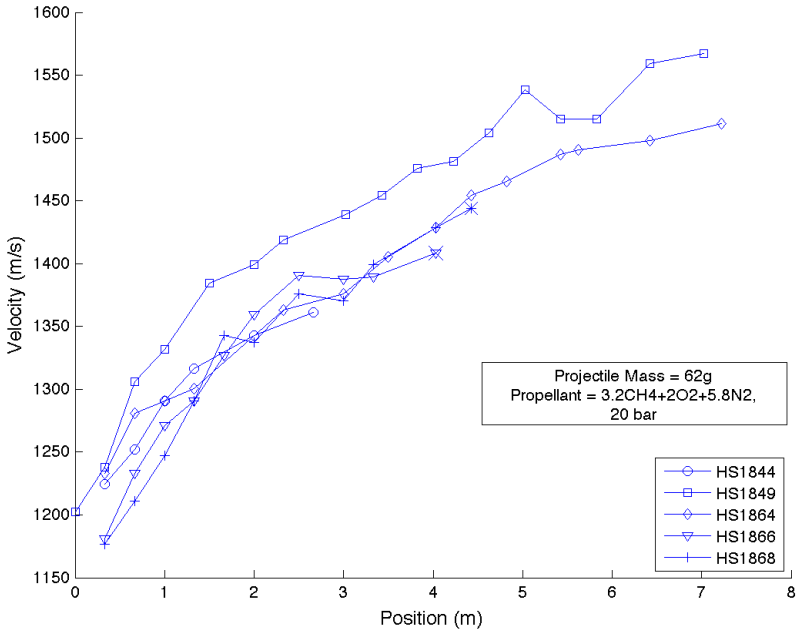

Figure 5.4: Velocity-distance data for successful tests using Type D polycarbonate projectiles

on the upper velocity limit, a polycarbonate projectile with a magnesium nose tip was tested (also shown in Figure 5.4). The propellant was adjusted to $3.1CH_4 + 2O_2 + 5.8N_2$. The change in CH_4 was done to mitigate observed inconsistency in

ignition in the $3.2CH_4 + 2O_2 + 5.8N_2$ propellant. In HS1866, a magnesium-tipped Type D projectile entered the test section at 1180 m/s and unstarted at 1410 m/s after 4 m. In a similar test, an aluminum-tipped polycarbonate projectile entered the $3.1CH_4 + 2O_2 + 5.8N_2$ test section at 1180 m/s and also unstarted at 1440 m/s after 4.4 m (HS1868). A magnesium-tipped polycarbonate projectile was also tested in a $2.7CH_4 + 2O_2 + 5.8N_2$ propellant at 25 bar to observe the effect of nosecone material on starting dynamics (a pure lexan projectile would not successfully start in $2.7CH_4 + 2O_2 + 5.8N_2$ mixture whereas the magnesium projectile would). This projectile promptly unstarted.

Tests were also performed in a two-stage ram accelerator configuration to find the upper velocity limit of the polycarbonate projectile, as shown in Figure 5.5. Here, a 3-m-long $3.2CH_4 + 2O_2 + 5.8N_2$ starter propellant was used followed by 7-m of $XCH_4 + 2O_2 + 2H_2 + 0.2He$ where X was either 6 or 6.5 moles. The initial test (HS1852) used a Type D polycarbonate projectile which entered the second stage of $6CH_4 + 2O_2 + 2H_2 + 0.2He$ at 1380 m/s and ran for 4.4 m before unstarting at 1470 m/s. Adjusting the propellant to $6.5CH_4 + 2O_2 + 2H_2 + 0.2He$ resulted in decreased performance (HS1853). The projectile entered the second stage 1340 and unstarted in less than a meter. A polycarbonate projectile was again modified to determine the effects of nosecone deformation on performance. A piece of 6.3 mm steel all-thread replaced the tip of the polycarbonate nose and was lathed down to match the 12.5° angle. This projectile drove further into the second stage, entering at 1380 m/s and accelerating to 1520 m/s in 2.6 m before unstarting, thus demonstrating an impact of nose tip material on peak velocity (HS1854).

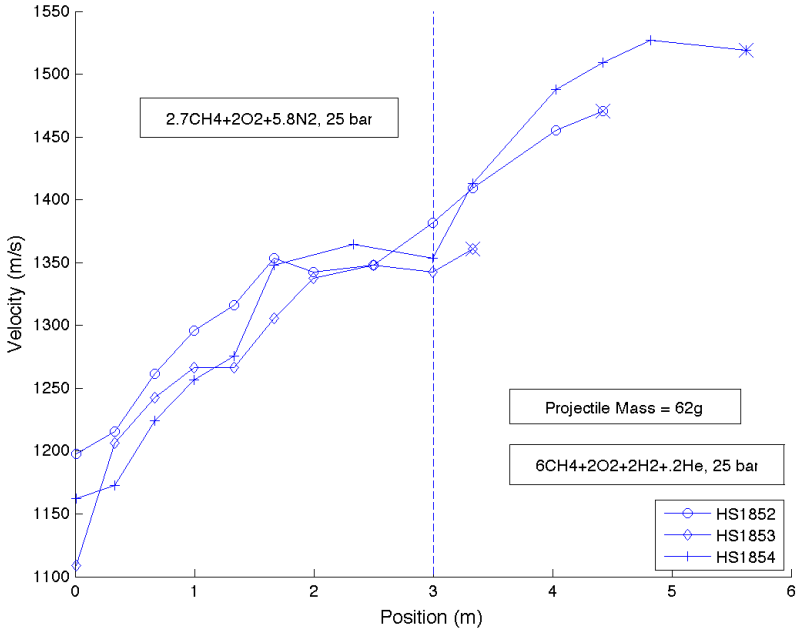

Figure 5.5: Velocity-distance data for two-stage tests using Type D polycarbonate projectile tests

5.2 Comparison with Theory

Experimental data from the upper velocity limit tests were also compared with theory. In Figure 5.6, the velocity-distance data for a magnesium projectile is plotted along with the corresponding theoretical performance prediction. Relatively good agreement with theory is observed past the transients associated with the ram accelerator starting process.

In Figure 5.7 theory is compared to experimental data for lexan projectiles. Here, the agreement with theory very poor. At the end of the 7 m run, the theory over predicts the velocity to be 1680 m/s compared to the experimental result of 1510 m/s, a difference of 11% which is much higher than the 1% discrepancy between theory and the magnesium projectile experiment.

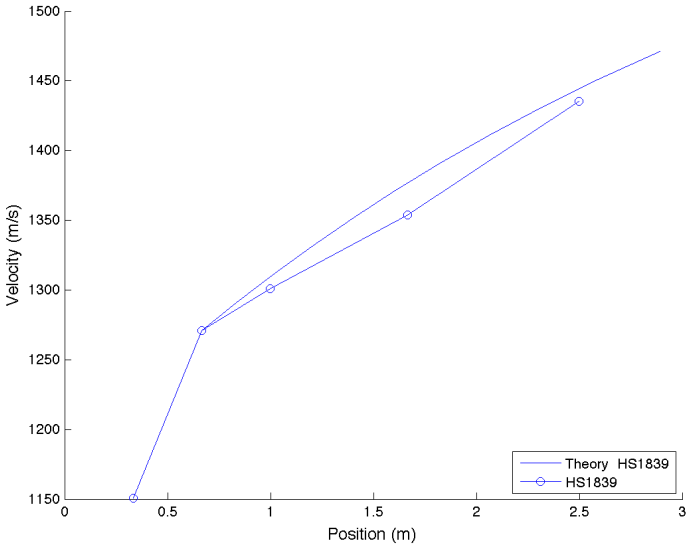

Figure 5.6: Theory vs. experimental data for magnesium projectile in a $2.7CH_4$ + $2O_2$ + $5.8N_2$ mixture

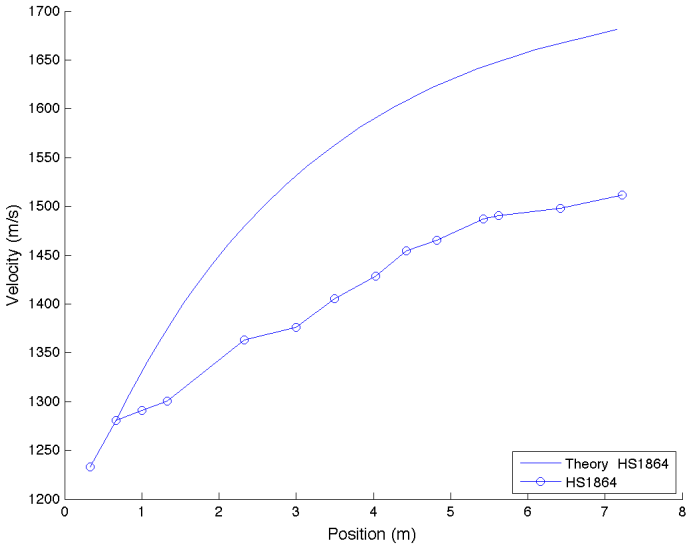

Figure 5.7: Theory vs. experimental data for Type D polycarbonate projectile in a $3.2CH_4$ + $2O_2$ + $5.8N_2$ mixture

5.3 Discussion

The inability of the polycarbonate projectile to start in the same propellant as the magnesium projectile was surprising because this was not the case in the low velocity starting tests. Changing the nose tip material to magnesium did not affect the results. Using the light gas gun, the mixture had to be cooled for the polycarbonate projectile to start. One possible explanation for this phenomenon is that the polycarbonate-polycarbonate interface between the obturator and projectile in these tests bonds differently than when using magnesium projectile, which might require more heat release in the propellant to displace the obturator. If this bond were a function of acceleration in the pre-launcher, its effect might not be present in the low velocity starting tests. Using an aluminum face plate between the projectile and obturator would test this theory but this experiment was not performed in this investigation.

The upper velocity limit of the polycarbonate projectiles was found to be significantly less than that of the magnesium projectiles. Magnesium projectiles traveled at velocities near 1800 m/s in a two stage ram accelerator test section and did not unstart in the test section. Polycarbonate projectiles in a similar two stage set-up unstarted almost immediately in the second stage. Replacing the polycarbonate nose tip with steel increased this distance to about 2.5 m and the projectile velocity reached about 1525 m/s, but this is still short of the velocity obtained by the magnesium projectile. One-stage ram accelerator tests with polycarbonate projectiles unstarted after about 7 m at around 1500 m/s. The improved performance of the polycarbonate projectile in the two stage configuration with the steel tip shows that the material of the nosecone does affect the upper velocity limit of the polycarbonate. The magnesium and aluminum tipped projectiles, however, demonstrated worse performance in the one-stage configuration than the all-polycarbonate projectiles. It is possible that the construction of the modified nose tips weakened the projectile and caused it to fail earlier than the all-polycarbonate projectile did.

Chapter 6

ANALYSIS OF MATERIAL EFFECTS

For all of the experiments, projectiles were made from polycarbonate or magnesium with properties listed in Table 6.1.

Table 6.1: Material properties

Material	Density (kg/m^3)	Yield Strength (Pa)	Melting Point (K)	Heat of Fusion (kJ/kg)	Thermal Conductivity (W/m-K)	Compressive Strength (MPa)
Polycarbonate	1250	$64.5x10^6$	430	130	0.2	80
Magnesium	1830	$2.5x10^8$	920	370	156	130

6.1 Heat Transfer

A computer code was written to analyze the heat transfer into the projectile wall during ram operation. The code solves the one dimensional heat equation (Equation 6.1) using a built-in partial differential equation solver in Matlab.

$$\frac{\partial u}{\partial t} = -\alpha \frac{\partial^2 u}{\partial x^2} \tag{6.1}$$

While the surface temperature of the projectile wall is calculated to be under the melting temperature of the material, a convective heat transfer boundary condition is used on the outer surface of the wall:

$$q_{convection} = q_{conduction} \tag{6.2}$$

$$hA(T_\infty - T_{surf}) = k\frac{\partial T}{\partial x} \tag{6.3}$$

The convective heat transfer coefficient h is calculated using

$$Nu = 0.023 Re_d^{0.8} Pr^{0.4} \tag{6.4}$$

and

$$Nu = \frac{hd}{k} \tag{6.5}$$

where Nu is the Nusselt number, Re_d is the Reynold's number based on diameter, Pr is the Prandtl number, d is the tube diameter, and k is the thermal conductivity. The temperature of the gas driving the heat transfer T_∞ is calculated from the stagnation temperature using

$$T_\infty = T\left(1 + \frac{\gamma - 1}{2} M^2\right) \tag{6.6}$$

where T is the static temperature of the gas. When the surface temperature reaches the melting temperature of the material, the boundary condition becomes a constant temperature condition, holding the surface temperature to the melting temperature:

$$T_{surf} = T_{melt} \tag{6.7}$$

The code assumes constant acceleration of the projectile throughout the ram test section starting from a velocity of 1100 m/s and ending at 2400 m/s over 16 m. In Figures 6.1 and 6.2 the temperature profile in the projectile wall is presented as a surface plot for magnesium and polycarbonate projectiles.

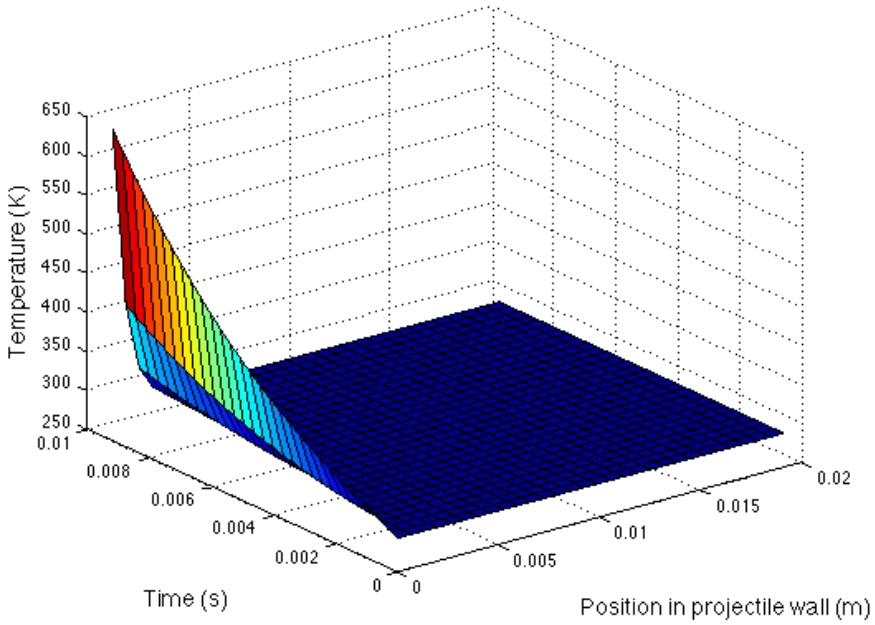

Figure 6.1: Temperature profile in wall of magnesium projectile over time

The polycarbonate reaches its melting temperature much more quickly than the magnesium, but the temperature disturbance does not propagate as deeply into the wall due to the polycarbonate's lower thermal conductivity.

To quantify the comparison between the two materials, a first order approximation of material loss was performed. The code was modified to calculate the rate of heat transfer into the projectile during test using

$$\dot{Q} = hA(T_\infty - T_{surf}) \tag{6.8}$$

This rate of heat transfer was integrated over the course of the run using a trapezoidal integration method. This total energy transfer was then divided by the heat of fusion for each material, yielding an estimated material loss. For the polycarbonate, the code predicted a loss of 0.479 kg per meter of wall length. For the magnesium,

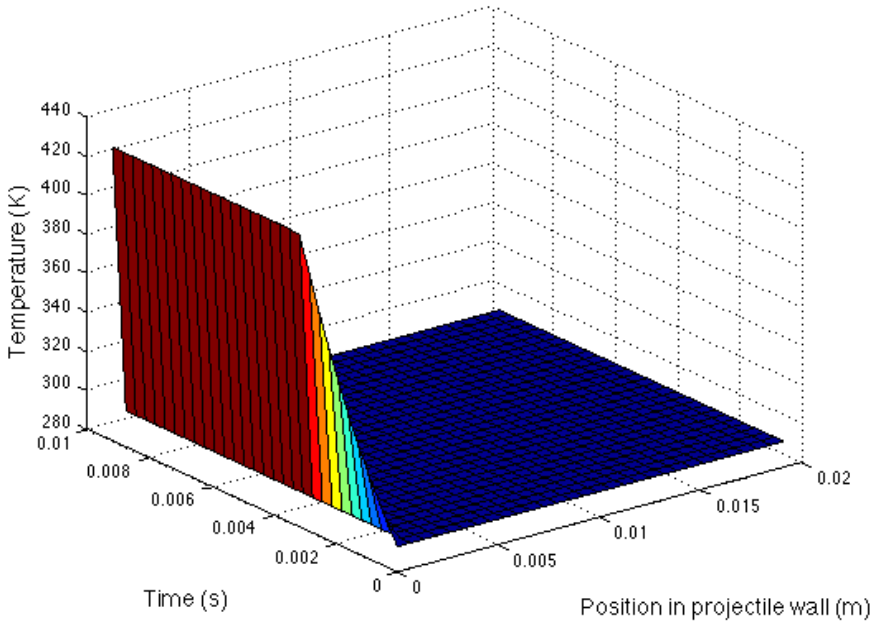

Figure 6.2: Temperature profile in wall of polycarbonate projectile over time

the loss was 0.147 kg per meter of wall length. For a projectile that is 130 mm long, this corresponds to a total loss of 0.062 kg for polycarbonate and 0.019 kg for magnesium. These values correspond to a a very higher percentage of starting projectile weight and clearly overestimate actual material losses. Nevertheless, they are useful to compare the two materials. The material loss of polycarbonate is predicted to be 3 times higher than that of a magnesium projectile. This phenomena could account for some of the performance differences observed in this experimental series.

6.2 Structural

A structural analysis was performed on a polycarbonate projectile. The purpose of the analysis was to identify the stresses in the projectile upon initial launch in the light gas gun or combustion gun before entering the ram test section. The structural analysis toolbox in Solidworks was used. Due to restrictions on mesh size and complexity,

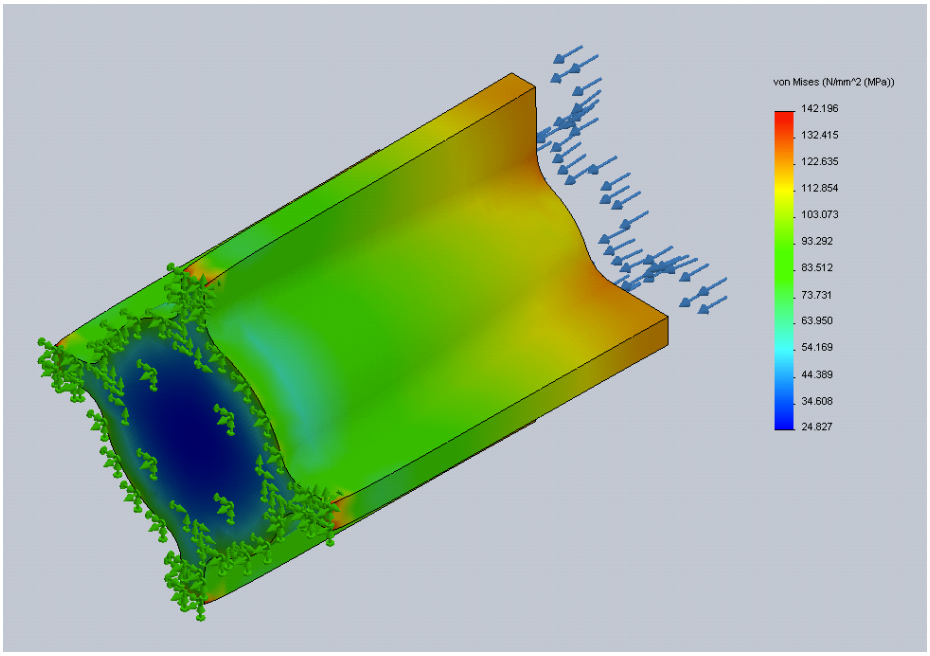

Figure 6.3: Von Mises Stress in polycarbonate projectile base under gun launch loading

only the base of the projectile was used in the model. The nosecone and leading edge of the fins were not included. The results from the analysis are in Figure 6.3.

The gun launch was simulated by calculating the force exerted by a full-bore obturator when it is subjected to typical launch pressures of 415 bar. The front of the truncated projectile was subjected to a zero displacement boundary condition. The maximum stress predicted is 140 MPa in the center of the projectile body and most of the base is well above the compressive strength of 80 MPa. These results are consistent with deformation observed in recovered polycarbonate projectiles. A buckling analysis would likely be the most appropriate way of predicting the deformation of the polycarbonate projectiles, but that was not performed in this investigation.

Chapter 7

CONCLUSION

The results of an investigation on the performance of polycarbonate projectiles in the ram accelerator were presented in this thesis. The investigation was divided into two series: low velocity starting and upper velocity limits. The low velocity starting tests were motivated by the need to reduce the burden on the initial launcher and to take full advantage of the ram accelerator low acceleration capabilities. Polycarbonate projectiles were successfully started at 810 m/s in a $1.75C_2H_6 + 3.5O_2 + 10.5CO_2$ propellant at 20 bar fill pressure . This lower velocity limit was the same one found for magnesium projectiles of the same geometry. Increasing the body length of the polycarbonate projectile, however, caused difficulties in starting and the starting velocity for this geometry was higher. The series of tests performed for low velocity starting used a new prelauncher based on a combustion wave cycle in which a hydrogen-oxygen propellant was detonated in the breech, providing a light, high temperature, driving gas.

The upper velocity limit testing revealed a velocity limit for the polycarbonate projectiles that was different from that of magnesium projectiles. Magnesium projectiles were able to reach velocities of approximately 1800 m/s before unstarting, whereas polycarbonate projectiles unstarted around 1550 m/s. Tests were run in both one-stage and two-stage configurations. Attempts were made to increase this velocity limit by installing metallic (magnesium, aluminum, or steel) nosecone tips on the polycarbonate projectiles. In a two-stage configuration, this change resulted in the projectile driving further before unstarting. In the one-stage configuration, this change resulted in a decreased velocity limit. The upper velocity limit tests used the

light gas gun that has been used in most of the testing at the UW facility. These tests also revealed an effect of projectile material on starting that was not present in the low velocity starting experiments. The heat release of the propellant had to be reduced from that used with magnesium projectiles to successfully start polycarbonate projectiles. It is possible that this is due to an interaction between the polycarbonate projectile and obturator that is not present when using magnesium projectiles.

7.1 Future Work

- Lower velocity starting: computational work has been done to investigate the possibility of "zero velocity starting" where a projectile is accelerated from rest using a ram accelerator. This technique would use a diaphragm containing propellant to burst ahead of the projectile, causing the propellant to flow towards it. If combustion can be sustained behind the projectile, it would accelerate. This concept could also be used to lower the required entrance velocity for the usual ram accelerator configuration. If a projectile is launched conventionally, prebreaking the entrance diaphragm ahead of it would provide flow of the propellant against its direction of travel. This superimposed flow could allow the projectile to start even if it is traveling below the Kantrowitz velocity. [18]

- Modifications to polycarbonate projectiles: The results from experiments using polycarbonate projectiles with aluminum, magnesium, and steel nosecone tips were inconsistent. Whereas a steel nose tip increased the upper velocity limit of a polycarbonate projectile in a two-stage ram accelerator configuration, the projectile experienced decreased performance in the one-stage configuration. The fact that both aluminum and magnesium nose tips had this result suggests that the construction of the modified projectile was the problem, not the nosetip's material. Thus, the experiments in the one-stage ram accelerator did not answer the question of nosecone tip material in a satisfactory manner. More work

should be done to determine if the nosecone (or other geometry features such as fins) is responsible for the polycarbonate projectile failing.

- Performance in other operating modes and velocity regimes: The experiments reported in this thesis were all done in the subdetonative velocity regime. Further investigations should be done on the performance of polycarbonate projectiles in higher velocity regimes and different operating modes that near the Chapman-Jouguet speed (transdetonative) and exceed the Chapman-Jouguet speed (superdetonative).

BIBLIOGRAPHY

[1] D.W. Bogdanoff. Ram accelerator direct space launch system: New concepts. *Journal of Propulsion and Power*, 8(2):481–490, March 1992.

[2] D.W. Bogdanoff, C. Knowlen, D. Murakami, and I. Stonich. Magnetic detector for projectiles in tubes. *AIAA Journal*, 28(11):1942–1944, December 1989.

[3] A.P. Bruckner, C. Knowlen, A. Hertzberg, and D.W. Bogdanoff. Operational characteristics of the thermally choked ram accelerator. *Journal of Propulsion and Power*, 7(5):828–836, September 1991.

[4] E.A. Burnham, A.E. Kull, C. Knowlen, A.P. Bruckner, and A. Hertzberg. Operation of the ram accelerator in the transdetonative velocity regime. In *26th Joint Propulsion Conference*, Orlando, FL, July 1990. AIAA/ASME/SAE/ASEE.

[5] G. Chew. *Projectile Nose Heating in the Ram Accelerator*. PhD thesis, University of Washington, 1995.

[6] E.C. Christofferson. A magnetic transducer detection system for high speed projectiles in tubes. Master's thesis, University of Washington, 1989.

[7] B. Dunmire. An experimental and theoretical investigation of single stage ram accelerator performance with emphasis towards projectile material effects. Master's thesis, University of Washington, 1991.

[8] A. Hertzberg, A.P. Bruckner, and D.W. Bogdanoff. Ram accelerator: A new chemical method for accelerating projectiles to ultrahigh velocities. *AIAA Journal*, 26(2):195–203, February 1988.

[9] A. Hertzberg, A.P. Bruckner, and C. Knowlen. Experimental investigation of ram accelerator propulsion modes. *Shock Waves*, 1:17–25, December 1991.

[10] A.J. Higgins. Gas dynamic limits of the ram accelerator. Master's thesis, University of Washington, 1993.

[11] A.J. Higgins, C. Knowlen, and A.P. Bruckner. Ram accelerator operating limits, part 1: Identification of limits. *Journal of Propulsion and Power*, 14(6):951–958, 1998.

[12] A.J. Higgins, C. Knowlen, and A.P. Bruckner. Ram accelerator operating limits, part 2: Nature of observed limits. *Journal of Propulsion and Power*, 14(6):959–966, 1998.

[13] T.S. Imrich. The impact of projectile geometry on ram accelerator performance. Master's thesis, University of Washington, 1995.

[14] C. Knowlen. *Theoretical and Experimental Investigation of the Thermodynamics of the Thermally Choked Ram Accelerator*. PhD thesis, University of Washington, April 1991.

[15] C. Knowlen, C. Bundy, A.P. Bruckner, and D. Kruczynski. Investigation of obturator and ignitor effects on low velocity starting of the ram accelerator. *Journal de Physique IV*, 10(11):49–58, 2000.

[16] C. Knowlen, J.G. Li, J. Hinkey, and B. Dunmire. University of washington ram accelerator facility. In *42nd Meeting of the Aeroballistic Range Association*, Adelaide, Australia, October 1991. Aeroballistic Range Association.

[17] C. Knowlen, E. Schultz, and A.P. Bruckner. Investigation of low velocity starting techniques for the ram accelerator. In *33rd Joint Propulsion Conference and Exhibit*, Seattle, WA, July 1997. AIAA/ASME/SAE/ASEE.

[18] K.A. McFall, C. Knowlen, A.P. Bruckner, and A. Hertzberg. Numerical analysis of zero velocity start technique for the ram accelerator. In *32nd Joint Propulsion Conference and Exhibit*, Lake Buena Vista, FL, July 1996. AIAA/ASME/SAE/ASEE.

[19] E. Schultz, C. Knowlen, and A.P. Bruckner. Starting envelope of the subdetonative ram accelerator. *Journal of Propulsion and Power*, 16(6):1040–1052, November 2000.

[20] J.F. Stewart, C. Knowlen, and A.P. Bruckner. Effects of launch tube gases on starting of the ram accelerator. In *33rd Joint Propulsion Conference and Exhibit*, Seattle, WA, July 1997. AIAA/ASME/SAE/ASEE.

Appendix A

LOW VELOCITY START EXPERIMENT SUMMARIES

CG = Combustion Gun

PC = Polycarbonate

SDU = Sonic Diffuser Unstart

WFO = Wave Fall Off

WU = Wave Unstart

Table A.1: Summary of Low Velocity Start Experiments

HS #	Body Length (mm)	Material	Gun type	Mixture	Fill Pres (bar)	V_{in} (m/s)	M_{in}	Start?	V_{max} (m/s)	M_{max}	Failure Mode
1749	48	Al	CG	2.7CH4+2O2+5.8N2	26	440	1.21	No	–	–	SDU
1750	48	Al	CG	2.7CH4+2O2+5.8N2	25	940	2.59	No	–	–	SDU
1751	48	Al	CG	2.7CH4+2O2+5.8N2	26	1110	3.05	No	–	–	WFO
1752	48	Al	CG	2.5CH4+2O2+5.8N2	26	–	–	No	–	–	Obt destroyed
1753	48	Al	CG	2.5CH4+2O2+5.8N2	26	–	–	No	–	–	Obt destroyed
1754	48	Al	CG	2.63C2H6+3.5O2+8.75CO2	26	610	2.13	No	–	–	SDU
1755	48	Al	CG	2.63C2H6+3.5O2+8.75CO2	26	380	1.33	No	–	–	SDU
1756	48	Al	CG	2.63C2H6+3.5O2+8.75CO2	26	750	2.62	No	–	–	SDU
1757	48	Al	CG	2.63C2H6+3.5O2+8.75CO2	26	800	2.80	No	–	–	WFO
1758	48	Al	CG	1.75C2H6+3.5O2+8.75CO2	26	760	2.66	No	–	–	WFO
1759	48	Mg	CG	1.75C2H6+3.5O2+8.75CO2	26	700	2.45	No	–	–	SDU

Continued on next page

Table A.1 – continued from previous page

HS #	Body Length (mm)	Material	Gun type	Mixture	Fill Pres (bar)	V_{in} (m/s)	M_{in}	Start?	V_{max} (m/s)	M_{max}	Failure Mode
1760	48	Mg	CG	1.75C2H6+3.5O2+8.75CO2	26	690	2.42	No	–	–	SDU
1761	48	Mg	CG	1.75C2H6+3.5O2+8.75CO2	26	940	3.30	No	–	–	WU
1762	48	Mg	CG	1.75C2H6+3.5O2+10.5CO2	26	820	2.91	No	–	–	WFO
1762	48	Mg	CG	1.75C2H6+3.5O2+10.5CO2	26	820	2.91	No	–	–	WFO
1763	48	Mg	CG	1.75C2H6+3.5O2+10.5CO2	26	870	3.09	Yes	1340	4.75	–
1764	48	Mg	CG	1.75C2H6+3.5O2+10.5CO2	25	830	2.94	Yes	1280	4.54	–
1765	48	Mg	CG	1.75C2H6+3.5O2+10.5CO2	26	750	2.66	No	–	–	SDU
1766	48	Mg	CG	1.75C2H6+3.5O2+10.5CO2	25	810	2.87	Yes	1220	4.33	–
1767	48	PC	CG	1.75C2H6+3.5O2+10.5CO2	26	820	2.91	No	–	–	WFO
1768	48	PC	CG	1.75C2H6+3.5O2+9.98CO2	26	890	3.14	No	–	–	SDU
1769	48	PC	CG	1.75C2H6+3.5O2+10.5CO2	20	–	–	No	–	–	WFO
1770	48	PC	CG	1.75C2H6+3.5O2+10.5CO2	17	900	3.19	Yes	995	3.53	–
1771	48	Mg	CG	1.75C2H6+3.5O2+10.5CO2	14	900	3.19	No	–	–	WU

Continued on next page

Table A.1 – continued from previous page

HS #	Body Length (mm)	Material	Gun type	Mixture	Fill Pres (bar)	V_{in} (m/s)	M_{in}	Start?	V_{max} (m/s)	M_{max}	Failure Mode
1772	48	Mg	CG	1.75C2H6+3.5O2+10.5CO2	14	700	2.48	No	–	–	SDU
1773	48	Mg	CG	1.75C2H6+3.5O2+10.5CO2	14	500	1.77	No	–	–	SDU
1774	48	Mg	CG	1.75C2H6+3.5O2+10.5CO2	26	1010	3.58	Yes	1260	4.47	–
1775	48	PC	CG	1.75C2H6+3.5O2+10.5CO2	24	1050	3.72	No	–	–	WU
1776	48	PC	CG	1.75C2H6+3.5O2+10.5CO2	14	1050	3.72	No	–	–	WU
1777	48	PC	CG	2.19C2H6+3.5O2+10.94CO2	14	1050	3.71	No	–	–	WU
1778	48	PC	CG	2.63C2H6+3.5O2+11.38CO2	14	1060	3.74	No	–	–	WFO
1779	48	PC	CG	2.19C2H6+3.5O2+10.94CO2	14	960	3.39	No	–	–	WU
1780	48	Mg	CG	1.75C2H6+3.5O2+10.5CO2	14	990	3.51	Yes	1210	4.29	–
1781	48	PC	CG	2.19C2H6+3.5O2+10.94CO2	14	–	–	No	–	–	WFO
1782	48	PC	CG	1.75C2H6+3.5O2+10.5CO2	14	1070	3.79	Yes	1180	4.18	–
1783	48	PC	CG	1.75C2H6+3.5O2+10.5CO2	14	800	2.84	No	–	–	WFO
1784	48	PC	CG	1.31C2H6+3.5O2+10.06CO2	14	790	2.79	No	–	–	WFO

Continued on next page

Table A.1 – continued from previous page

HS #	Body Length (mm)	Material	Gun type	Mixture	Fill Pres (bar)	V_{in} (m/s)	M_{in}	Start?	V_{max} (m/s)	M_{max}	Failure Mode
1785	48	PC	CG	1.31C2H6+3.5O2+9.63CO2	17	820	2.89	No	–	–	WU
1786	48	PC	CG	1.75C2H6+3.5O2+10.5CO2	17	860	3.05	No	–	–	WFO
1787	48	PC	CG	1.75C2H6+3.5O2+10.5CO2	21	860	3.05	Yes	1175	4.17	–
1788	48	PC	CG	1.75C2H6+3.5O2+10.5CO2	21	810	2.87	Yes	1150	4.08	–
1789	48	PC	CG	1.75C2H6+3.5O2+10.5CO2	21	750	2.66	No	–	–	WFO
1790	132	PC	CG	1.75C2H6+3.5O2+10.5CO2	21	850	3.01	No	–	–	WFO
1791	91	PC	CG	1.75C2H6+3.5O2+10.5CO2	21	860	3.05	No	–	–	WFO
1792	91	PC	CG	1.75C2H6+3.5O2+10.5CO2	24	870	3.09	Yes	1055	3.74	–
1793	132	PC	CG	1.75C2H6+3.5O2+10.5CO2	24	860	3.05	No	–	–	WFO
1794	132	PC	CG	1.75C2H6+3.5O2+9.63CO2	24	850	2.99	No	–	–	WU
1795	91	PC	CG	1.75C2H6+3.5O2+10.5CO2	24	840	2.98	No	–	–	WU
1796	91	PC	CG	1.75C2H6+3.5O2+10.5CO2	24	850	3.01	Yes	1190	4.22	–
1797	91	PC	CG	1.75C2H6+3.5O2+10.5CO2	24	840	2.98	Yes	1000	3.55	WU

Continued on next page

Table A.1 – continued from previous page

HS #	Body Length (mm)	Material	Gun type	Mixture	Fill Pres (bar)	V_{in} (m/s)	M_{in}	Start?	V_{max} (m/s)	M_{max}	Failure Mode
1798	91	PC	CG	2C2H6+3.5O2+14CO2	24	810	2.87	No	–	–	WFO
1799	91	PC	CG	1.86C2H6+3.5O2+11.17CO2	24	910	3.22	Yes	1180	4.17	–
1800	91	PC	CG	1.86C2H6+3.5O2+11.17CO2	24	870	3.08	No	–	–	WFO
1801	91	PC	CG	1.86C2H6+3.5O2+11.17CO2	24	920	3.25	No	1010	3.57	WU
1802	91	PC	CG	1.86C2H6+3.5O2+11.17CO2	24	900	3.18	No	–	–	WU
1803	91	PC	CG	1.86C2H6+3.5O2+11.17CO2	24	900	3.18	No	–	–	WFO
1804	91	PC	CG	1.86C2H6+3.5O2+11.17CO2	24	900	3.18	No	–	–	WU
1805	91	PC	CG	1.86C2H6+3.5O2+11.63CO2	24	950	3.36	Yes	1212	4.29	–
1806	91	PC	CG	1.86C2H6+3.5O2+11.63CO2	24	920	3.26	No	–	–	WFO
1807	91	PC	CG	1.86C2H6+3.5O2+11.63CO2	24	910	3.22	No	–	–	WU
1808	91	PC	CG	1.5C2H4+3O2+12CO2	25	930	3.30	No	–	–	WFO
1809	91	PC	CG	1.5C2H4+3O2+10CO2	25	940	3.31	No	–	–	WU
1810	91	PC	CG	1.5C2H4+3O2+11CO2	25	890	3.14	No	–	–	WU

Continued on next page

Table A.1 – continued from previous page

HS #	Body Length (mm)	Material	Gun type	Mixture	Fill Pres (bar)	V_{in} (m/s)	M_{in}	Start?	V_{max} (m/s)	M_{max}	Failure Mode
1811	91	PC	CG	1.5C2H4+3O2+11.5CO2	25	910	3.22	No	–	–	WFO
1812	91	PC	CG	1.5C2H4+3O2+11.5CO2	25	900	3.18	No	–	–	WU
1813	91	PC	CG	1.5C2H4+3O2+12CO2	25	910	3.22	No	–	–	WU
1814	91	PC	CG	1.5C2H4+3O2+11.5CO2	21	940	3.33	Yes	1310	4.64	–
1815	91	PC	CG	1.5C2H4+3O2+11.5CO2	20	950	3.36	No	–	–	WU
1816	91	PC	CG	1.5C2H4+3O2+11.5CO2	21	940	3.33	Yes	1310	4.64	–
1817	91	PC	CG	1.5C2H4+3O2+11.5CO2	21	940	3.33	Yes	1230	4.35	–
1818	91	PC	CG	1.5C2H4+3O2+11.5CO2	21	930	3.29	No	–	–	WFO
1819	91	PC	CG	1.5C2H4+3O2+11.1CO2	21	930	3.29	No	–	–	WU
1820	91	PC	CG	1.5C2H4+3O2+11.5CO2	21	790	2.80	No	–	–	WFO
1821	91	PC	CG	1.5C2H4+3O2+9.5CO2	21	770	2.70	No	–	–	WU
1822	91	PC	CG	1.5C2H4+3O2+9.5CO2	21	930	3.27	No	–	–	WU
1823	91	PC	CG	1.5C2H4+3O2+12CO2	24	940	3.33	No	–	–	WU

Continued on next page

Table A.1 – continued from previous page

HS #	Body Length (mm)	Material	Gun type	Mixture	Fill Pres (bar)	V_{in} (m/s)	M_{in}	Start?	V_{max} (m/s)	M_{max}	Failure Mode
1824	91	PC	CG	1.5C2H4+3O2+12.5CO2	24	930	3.30	No	–	–	WU
1825	91	PC	CG	1.5C2H4+3O2+13CO2	24	730	2.59	No	–	–	SDU
1826	91	PC	CG	1.5C2H4+3O2+13CO2	24	890	3.16	No	–	–	WU
1827	91	PC	CG	1.5C2H4+3O2+14CO2	24	900	3.21	No	–	–	WFO
1828	91	PC	CG	1.5C2H4+3O2+13.5CO2	24	920	3.27	Yes	1140	4.06	–
1829	91	PC	CG	1.5C2H4+3O2+13.5CO2	24	850	3.02	No	–	–	SDU
1830	91	PC	CG	1.5C2H4+3O2+13.5CO2	24	890	3.17	No	–	–	WU

Appendix B

UPPER VELOCITY LIMIT EXPERIMENT SUMMARIES

CG = Combustion Gun

LGG = Light Gas Gun

PC = Polycarbonate

SDU = Sonic Diffuser Unstart

WFO = Wave Fall Off

WU = Wave Unstart

Table B.1: Summary of Upper Velocity LimitExperiments

HS #	Material	Gun type	Mixture	Fill Pres (bar)	V_{in} (m/s)	M_{in}	Start?	Drive / Stage length (m)	V_{max} (m/s)	M_{max}	Failure Mode
1831	Mg	CG	2.7CH4+2O2+5.8N2	24	870	2.39	No	–	–	–	SDU
1832	Mg	CG	2.7CH4+2O2+5.8N2	24	980	2.70	No	–	–	–	SDU
1833	PC	CG	2.7CH4+2O2+5.8N2	24	1150	3.17	No	–	–	–	WU
1834	PC	CG	2.7CH4+2O2+5.8N2	24	1090	3.00	No	–	–	–	WU
1835	PC	CG	2.7CH4+2O2+6.8N2	24	1030	2.84	No	–	–	–	SDU
1836	PC	CG	2.7CH4+2O2+6.8N2	24	1140	3.15	No	–	–	–	SDU
1837	PC	CG	3.2CH4+2O2+6.8N2	24	1220	3.33	No	–	–	–	WU
1838	PC	CG	3.7CH4+2O2+6.8N2	24	1070	2.92	No	–	–	–	WU
1839	Mg	LGG	2.7CH4+2O2+5.8N2	23	1150	3.17	Yes	3/3	1500	4.13	–
1840	Mg	LGG	2.7CH4+2O2+5.8N2/ 6CH4+2O2+2H2+0.2He	19/19	1190	3.28	Yes	16/16	1810	4.00	–
1841	PC	LGG	2.7CH4+2O2+5.8N2	19	1280	3.52	No	–	–	–	WU

Continued on next page

Table B.1 – continued from previous page

HS #	Material	Gun type	Mixture	Fill Pres (bar)	V_{in} (m/s)	M_{in}	Start?	Drive / Stage length (m)	V_{max} (m/s)	M_{max}	Failure Mode
1842	PC	LGG	2.7CH4+2O2+5.8N2	21	1230	3.39	No	–	–	–	WU
1843	PC	LGG	2.7CH4+2O2+5.8N2	16	1130	3.11	No	–	–	–	WU
1844	PC	LGG	3.2CH4+2O2+5.8N2	22	1220	3.33	Yes	3/3	1380	3.77	–
1845	PC	LGG	3.2CH4+2O2+5.8N2	23	1220	3.33	Yes	3/3	1370	3.74	–
1846	PC	LGG	3.2CH4+2O2+5.8N2/ 6CH4+2O2+2H2+0.2He	19/25	1200	3.28	Yes	3/16	1310	–	SDU in 2nd stg
1847	PC	LGG	3.2CH4+2O2+5.8N2/ 6CH4+2O2+2H2+0.2He	22/23	1220	3.33	Yes	2/16	1330	3.63	WU in 1st stg
1848	PC	LGG	3.2CH4+2O2+5.8N2/ 6CH4+2O2+2H2+0.2He	25/25	1220	3.33	Yes	2/15	1340	3.66	WU in 1st stg
1849	PC	LGG	3.2CH4+2O2+5.8N2	23	1220	3.33	Yes	7/7	1560	4.26	SDU
1850	PC	LGG	3.2CH4+2O2+5.8N2/ 6CH4+2O2+2H2+0.2He	23/20	1190	3.25	No	–	–	–	–

Continued on next page

Table B.1 – continued from previous page

HS #	Material	Gun type	Mixture	Fill Pres (bar)	V_{in} (m/s)	M_{in}	Start?	Drive / Stage length (m)	V_{max} (m/s)	M_{max}	Failure Mode
1851	PC	LGG	3.2CH4+2O2+5.8N2/ 6CH4+2O2+2H2+0.2He	25/25	1190	3.25	No	–	–	–	SDU
1852	PC	LGG	3.2CH4+2O2+5.8N2/ 6CH4+2O2+2H2+0.2He	25/22	1200	3.28	Yes	4.5/8	1470	3.24	WU in 2nd stg
1853	PC	LGG	3.2CH4+2O2+5.8N2/ 6.5CH4+2O2+2H2+0.2He	26/25	1110	3.03	Yes	3/10	1360	3.00	WU in 2nd stg
1854	PC, steel nose tip	LGG	3.2CH4+2O2+5.8N2/ 6CH4+2O2+2H2+0.2He	26/25	1160	3.17	Yes	5/10	1530	3.38	WU in 2nd stg
1855	PC, Mg nose tip	LGG	3.2CH4+2O2+5.8N2/ 6CH4+2O2+2H2+0.2He	26/25	1180	3.22	Yes	3/10	1440	3.18	WU in 2nd stg
1856	Mg	LGG	2.7CH4+2O2+5.8N2/ 6CH4+2O2+2H2+0.2He	26/26	1100	3.03	No	–	–	–	SDU

Continued on next page

Table B.1 – continued from previous page

HS #	Material	Gun type	Mixture	Fill Pres (bar)	V_{in} (m/s)	M_{in}	Start?	Drive / Stage length (m)	V_{max} (m/s)	M_{max}	Failure Mode
1857	Mg	LGG	2.7CH4+2O2+5.8N2/ 6CH4+2O2+2H2+0.2He	26/26	1170	3.22	Yes	2/16	1350	3.72	WU in 1st stg
1858	Mg	LGG	2.7CH4+2O2+5.8N2/ 6CH4+2O2+2H2+0.2He	25/25	1160	3.19	Yes	12/16	1840	4.06	WU in 2nd stg
1859	Mg	LGG	2.7CH4+2O2+5.8N2/ 5CH4+2O2+2H2	26/25	1130	3.11	Yes	8/16	1840	4.06	WU in 2nd stg
1860	PC, Mg nose tip	LGG	2.7CH4+2O2+5.8N2/ 5CH4+2O2+2H2+0.2He	26/25	1180	3.25	No	–	–	–	WU
1861	Mg	LGG	2.7CH4+2O2+5.8N2/ 5CH4+2O2+2H2+0.2He	25/26	1100	3.03	No	–	–	–	SDU
1864	PC	LGG	3.2CH4+2O2+5.8N2	23	1230	3.36	Yes	7/16	1510	4.13	WU
1865	PC, Mg nose tip	LGG	3.2CH4+2O2+5.8N2	23	1150	3.14	No	–	–	–	WFO

Continued on next page

Table B.1 – continued from previous page

HS #	Material	Gun type	Mixture	Fill Pres (bar)	V_{in} (m/s)	M_{in}	Start?	Drive / Stage length (m)	V_{max} (m/s)	M_{max}	Failure Mode
1866	PC, Mg nose tip	LGG	3.2CH4+2O2+5.8N2	23	1180	3.22	Yes	4/10	1410	3.85	WU
1868	PC, Al nose tip	LGG	3.2CH4+2O2+5.8N2	23	1180	3.22	Yes	4/10	1440	3.93	WU